



SCHOOL of
GRADUATE STUDIES
EAST TENNESSEE STATE UNIVERSITY

East Tennessee State University
Digital Commons @ East
Tennessee State University

Electronic Theses and Dissertations


Student Works

5-2017

Functionalized Silica Gel for Adsorption of Cesium from Solution

Kenneth Marshall Seaton III
East Tennessee State University

Follow this and additional works at: <https://dc.etsu.edu/etd>

 Part of the [Analytical Chemistry Commons](#), [Environmental Chemistry Commons](#), [Inorganic Chemistry Commons](#), and the [Materials Chemistry Commons](#)

Recommended Citation

Seaton, Kenneth Marshall III, "Functionalized Silica Gel for Adsorption of Cesium from Solution" (2017). *Electronic Theses and Dissertations*. Paper 3215. <https://dc.etsu.edu/etd/3215>

This Thesis - Open Access is brought to you for free and open access by the Student Works at Digital Commons @ East Tennessee State University. It has been accepted for inclusion in Electronic Theses and Dissertations by an authorized administrator of Digital Commons @ East Tennessee State University. For more information, please contact digilib@etsu.edu.

Functionalized Silica Gel for Adsorption of
Cesium from Solution

A thesis
presented to
the faculty of the Department of Chemistry
East Tennessee State University

In partial fulfillment
of the requirements for the degree
Master of Science in Chemistry

by
Kenneth Marshall Seaton III
May 2017

Dr. Aleksey Vasiliev, Chair
Dr. Greg Bishop
Dr. Marina Roginskaya

Keywords: Sol-gel synthesis, adsorption, phosphotungstic acid, cation exchange, cesium removal

ABSTRACT

Functionalized Silica Gel for Adsorption of Cesium from Solution

by

Kenneth Marshall Seaton III

Mesoporous silica gel containing embedded phosphotungstic acid (PTA) was synthesized by sol-gel co-condensation of tetraethyl orthosilicate with PTA in acidic media. The obtained material had high Brunauer-Emmett-Teller Theory (BET) surface area and pore volume. A characteristic band of the Keggin structure of PTA was present in its FT-IR spectrum while its X-ray diffraction patterns were absent. This proved the embedding of PTA on a sub-molecular level and not as a second phase. Acidic sites were determined by neutralization with base in aprotic solvent, followed by titration of the remaining base with an acid. The material demonstrated high adsorption capacity of Cs. Kinetic studies showed that the adsorption data correlates strongly with the pseudo-second order model. At higher temperatures, the nature of adsorption fit the Langmuir model extremely well. The obtained results can be used in the development of an effective adsorbent for clean-up of water contaminated by radioactive ^{137}Cs .

DEDICATION

This work is dedicated to my Aunt Rebecca, Uncle Coy, Aunt Stephanie, Uncle Dale, my cousins Frankie Sparks and Alex Sparks, my brother Joseph Seaton, my friends Zachary Larison and Jacob Decima, and to my grandmother Shirley Sparks.

ACKNOWLEDGEMENTS

I would like to thank Dr. Vasiliev for being so patient and understanding during my journey through graduate school, and for the being the best advisor I could ask for.

My deepest appreciation goes out to Dr. Kirkby and Dr. Roginskaya for dealing with my constant barrage of questions and always offering to help when I had them.

Thank you Dr. Bishop for helping me develop a stronger foundation in analytical instrumentation for use in my research.

Thank you Dr. Mohseni for helping with the use of instrumentation, it wouldn't have been possible without your help.

This research was sponsored by NATO's Emerging Security Challenges Division in the framework of the Science for Peace and Security Programme (grant SfP 984639).

TABLE OF CONTENTS

	Page
ABSTRACT	2
DEDICATION.....	3
ACKNOWLEDGEMENTS.....	4
LIST OF TABLES	8
LIST OF FIGURES	9
LIST OF ABBREVIATIONS.....	11
Chapter	
1. INTRODUCTION.....	12
Danger of Radioactive Cesium	12
Cesium Removal	14
Heteropolyacids	17
Incorporation of Heteropolyacids to Silica Gel.....	20
2. EXPERIMENTAL / METHODOLOGY	25
Materials Used.....	25
Synthetic Methods	25
Instrumental Characterization	26
Elemental Analysis	26
Surface Acidity	26
Spectral Analysis	27

Structure and Morphology.....	27
Thermal Analysis	28
Adsorption.....	29
Batch Tests	29
Kinetic Studies.....	30
Column Tests.....	31
3. RESULTS AND DISCUSSION.....	32
Synthesis and Composition.....	32
Instrumental Characterization	33
FT-IR Spectroscopy	33
Solid State NMR Spectroscopy	34
Surface Acidity	36
TEM Imaging	38
Porosity.....	39
Particle Size	40
X-Ray Diffraction.....	41
Thermoanalysis.....	42
Adsorption Studies	44
Adsorption of Cesium	44
Selectivity.....	47
Adsorption of Strontium and Cobalt.....	48
Diffusion Study.....	49
Column Adsorption Tests.....	52

Discussion	54
Conclusions	57
REFERENCES	58
VITA	65

LIST OF TABLES

Table	Page
1. Characteristics of H-PTA/SiO ₂ and Cs-PTA/SiO ₂	32
2. Parameters of Adsorption	45
3. Diffusion and Kinetics Data.....	49

LIST OF FIGURES

Figure	Page
1. The Keggin structure of $H_3PW_{12}O_{40}$	17
2. The acid-catalyzed polycondensation of TEOS.....	22
3. The formation of a porous system using a surfactant in sol-gel synthesis	23
4. FT-IR spectra of H-PTA/SiO ₂ and Cs-PTA/SiO ₂	33
5. Solid state NMR spectra of H-PTA/SiO ₂ and Cs-PTA/SiO ₂	35
6. Titration curves for blank solution (1), 0.1 g Cs-PTA/SiO ₂ (2) and 0.1 g H-PTA/SiO ₂ (3) with pyridine (a) and diphenylamine (b).....	37
7. TEM images of H-PTA/SiO ₂ (a and b) and Cs-PTA/SiO ₂ (c).....	38
8. Nitrogen adsorption isotherms (a) and pore size distribution (b) of H-PTA/SiO ₂ and Cs-PTA/SiO ₂	39
9. Particle size distribution of H-PTA/SiO ₂ and Cs-PTA/SiO ₂	40
10. XRD patterns of H-PTA/SiO ₂ and Cs-PTA/SiO ₂	42
11. DSC and TGA curves of H-PTA/SiO ₂	43
12. Adsorption of Cs ⁺ by H-PTA/SiO ₂ (a) and linear fitting plots of Langmuir (b), Freundlich (c) and Temkin (d) isotherm models at 23, 31 and 39 °C	44
13. Effect of other alkali metals on Cs ⁺ adsorption on H-PTA/SiO ₂	47
14. Adsorption of Sr ²⁺ and Co ²⁺ on H-PTA/SiO ₂	48
15. Kinetics of Cs ⁺ adsorption at different initial concentrations (1 – 100, 2 – 200, 3 – 300, 4 – 400, 5 - 500 mg/L): amount adsorbed vs. time (a), diffusion rate (b), pseudo-first order fitting (c), pseudo-second order fitting (d)	50
16. Intraparticle diffusion rate constants at different Cs ⁺ concentrations	51

17. Cumulative adsorption of Cs ⁺ by H-PTA/SiO ₂ in CsCl solution flow at different initial concentrations (1 – 100, 2 – 200, 3 – 300, 4 – 400, 5 – 500 mg/L)	53
18. Dependence of the average adsorption rate on the initial Cs ⁺ concentration.....	54
19. Two types of active adsorption sites for Cs ⁺ : Silanol groups (1 – water-leachable, 2 – acid-leachable, 3 – base-leachable) and PTA (4 – non-leachable).....	56

LIST OF ABBREVIATIONS

AAS	Atomic Absorption Spectroscopy
BET	Brunauer-Emmett-Teller Theory
CuFC	Copper Ferrocyanide
DFT	Density Functional Theory
DSC	Differential Scanning Calorimetry
FT-IR	Fourier Transform Infrared Spectroscopy
HPA	Heteropolyacid
MNP	Magnetic Nanoparticles
NMR	Nuclear Magnetic Resonance
PB	Prussian Blue
PTA	Phosphotungstic Acid
Cs-PTA/SiO ₂	Cesium-Exchanged H-PTA-SiO ₂
H-PTA/SiO ₂	Phosphotungstic Acid Embedded in Silica Gel
S _N 2	Second-Order Nucleophilic Substitution
TEM	Transmission Electron Microscopy
TEOS	Tetraethyl Orthosilicate
TGA	Thermogravimetric Analysis
XRD	X-Ray Diffraction

CHAPTER 1

INTRODUCTION

Danger of Radioactive Cesium

Cesium, a member of the alkali metal family, has only one naturally occurring isotope, which is ^{133}Cs . Several radioisotopes of cesium exist, such as ^{135}Cs and ^{134}Cs , but one radioisotope of Cs is of particular danger: ^{137}Cs . ^{137}Cs is not produced naturally in any significant amount, but is a byproduct of nuclear fission in reactors and weapons testing. Due to nuclear weapons testing (which occurred up to the 1980's) and relatively recent industrial disasters, ^{137}Cs has been emitted into different layers of the atmosphere as well as the environments surrounding the release. To illustrate the danger resulting from ^{137}Cs contamination, if less than two grams of ^{137}Cs were to be distributed evenly over Central Park in New York, the zone would be considered a radioactive exclusion zone and therefore uninhabitable.¹ Recent nuclear accidents, namely the Chernobyl and Fukushima disasters, released high levels of radiation into the environment, up to $40,000 \text{ kBq m}^{-2}$ in the case of the Chernobyl incident.² Due to ^{137}Cs being the most abundant long-lived radionuclide released by nuclear reactors and having a half-life of approximately 30 years, the effects of its presence in the environment can be observed long after release.

Large-scale nuclear accidents are not the only source of ^{137}Cs , however. Numerous other small releases have been recorded in various parts of the world. Process accidents, which occur during fissile materials processing, have contributed to deaths and hospitalizations due to radiation exposure. Radiation therapy units contain ^{137}Cs and many hospitals use it to calibrate equipment, but irresponsible use or improper storage can lead to emission of harmful radiation,

resulting in hospitalization and sometimes death. Due to this possibility, the potential for ^{137}Cs to be used by terrorists exists and must be addressed accordingly. Exposure to high energy radiation from radionuclides results in irreversible damage to the human body, therefore measures to treat and effectively remove ^{137}Cs from the environment are extremely important.

Although ^{137}Cs itself, when concentrated in human tissue, can have adverse effects on the human body, it is the radiation the radioisotope emits that is of particular concern. ^{137}Cs degrades by very high-energy pathways, producing β and γ radiation.³ β radiation is lower in energy and is unable to penetrate through to the organs, while γ radiation passes through the entire body, resulting in radiative damage to tissue. However, when internally exposed to radiocesium, lower energy radiation can cause sufficient damage.³

An area of farmland in Japan was studied after radionuclide contamination by the Fukushima meltdown after the incident on March 11th, 2011, and the presence of radiocesium was subsequently monitored. It was found that rice from fields located in the Fukushima Prefecture retains radiocesium in concentrations that exceed the Japanese limit of 100 Bq kg^{-1} for grains.⁴ In addition, the factors related to soil-to-fruit transfer were studied by Velasco, *et al.* to demonstrate the potential for radiocesium to enter the human diet.⁵ Cesium exists in soil solutions as a hydrated cation with very little tendency to form insoluble complexes, having chemistry closely resembling that of potassium, resulting in high mobility and the potential to be absorbed by plant roots and translocated to other plant parts.⁵ The bioavailability and mobility of ^{137}Cs is of significant concern in the chemistry community due to the possibility of entering the food chain, and action must be taken to remedy the problem of radiocesium contamination in the environment.

Cesium Removal

Most compounds of cesium, like those of other alkali metals, are generally very soluble in aqueous media. Other radionuclides released into the atmosphere following nuclear accidents, such as ^{60}Co and ^{90}Sr , form very insoluble compounds with many different anions, making separation following their release relatively simple. The environmental mobility of the Cs^+ ion is very high, which causes the contaminant to be easily introduced into food or potable water. Due to other alkali metals' tendency to compete with cesium for adsorption sites, highly specific adsorbents are needed for effective removal.

Because the removal of cesium is inherently difficult, many people have tried to find solutions to this problem. Existing technologies and current research for removing ^{137}Cs from soil and water fall into five general categories: solvent extraction, phytoextraction, precipitation, ion exchange, and adsorption.⁶⁻⁸ However, the first four approaches have insufficient effectiveness due to low selectivity and high cost. The adsorption method has attracted a great deal of attention due to rapid separation, high thermal and radiation stabilities of the adsorbents, and reduced volume of wastes.

Inorganic adsorbents yield selective separation of trace radioactive nuclides in solutions containing a high concentration of salts. In addition, inorganic adsorbents exhibit several desirable properties including high thermal and radiation stability.⁹ A number of inorganic adsorbent materials have been investigated including natural and synthetic materials. Natural materials such as clay minerals, soils, sediments and rocks have shown adsorptive characteristics towards Cs, including pure minerals such as illite, kaolinite, montmorillonite, bentonite, magnesite, phlogopite, granite, sepiolite and goethite. In addition, zeolites including clinoptilolite, chabazite, and natural and synthetic mordenite have been applied in cesium

removal in wastewaters.⁹ Wagh *et al.* successfully synthesized a chemically bonded phosphate ceramic (ceramicrete) for nuclear waste immobilization and nuclear radiation shielding.¹⁰ To accomplish this, they partially replaced potassium by cesium in the struvite structure, thus forming a struvite-(K,Cs) mineral. Although these materials demonstrate reasonable adsorptive characteristics, they are not feasible for selective and efficient cesium removal due to the weak interaction between cesium and the elements on their surface.

Ferrocyanides exhibit adsorption properties desirable for cesium removal due to their high affinity for cesium as well as relative stability over a large range of pH. Ferrocyanides are generally prepared as either a grainy or powdered insoluble solid with reproducible chemical and physical properties.¹¹ One drawback, however, is that it is difficult to effectively use insoluble hexaferrocyanides on columns because they are composed of very small particles, which complicates the separation of saturated adsorbents from liquid waste. Han *et al.* used copper ferrocyanide (CuFC) as an adsorbent, but the CuFC particles used were very small.¹¹ This problem was solved by immobilizing CuFC on a support material such as silica gel, which can be modified to yield specific characteristics depending on the type of chemistry involved. However, the disadvantages accompanied by this approach included a reduced adsorption capacity of CuFC by the support materials and kinetics of adsorption being negatively affected.¹¹ Other methods of membrane separation used in treatment of cesium-containing liquid waste include nanofiltration, semipermeable dynamic membranes, ultra-filtration, and membrane distillation, but these generally are not as advantageous as the adsorption micro filtration process due to high pressures and energy consumptions.¹²

Arguably the most effective among the treatments using ferrocyanides is Prussian blue (PB). PB is a dark blue pigment with chemical formula $\text{Fe}_7(\text{CN})_{18}$ arranged in a face-center

lattice structure with eight water molecules existing in the unit cell. Pharmaceutical grade PB has been effectively used to remove cesium from the body of a patient after the Chernobyl disaster in 1987, as well as in the decontamination efforts after the Fukushima disaster, due to its high selectivity towards cesium.¹³ Nanoparticles of PB have been effectively synthesized in several cases and modified in order to yield more desirable characteristics.¹² Omura *et al.* successfully dispersed PB nanoparticles in water by modifying their surface.¹⁴ Using a spin-coating method, fabrication of a thin film with a water-dispersible ink of PB nanoparticles was achieved with a film thickness estimated at 40-430 nm.¹⁴ Nanocomposites based on functional silica or glass matrices containing PB nanoparticles of <10 nm have been shown to exhibit adsorption rates ten times higher than bulk analogues and three times higher adsorption capacity.¹⁵ Thammawong, *et al.* proposed that PB magnetic nanoparticles (MNP) could be used as an effective new type of drug for human body decontamination of cesium pollution. However, this approach has limited applicability in environmental chemistry due to the low recovery rate of MNP in drinking water streams.¹⁶ Chen, *et al.* applied a PB non-woven fabric in batch and column tests as a method to remove soluble cesium from waterworks.¹⁷ However, it was found that impurities in drinking waters such as humic substances, residual coagulants and residual chlorine could interfere with effective cesium removal.

Although ferrocyanides demonstrate a high degree of selectivity towards cesium with good adsorptive characteristics, these compounds decompose readily into harmful chemicals and, more importantly for the purpose of this work, are unstable under radiation. In order to successfully remove radioisotopes of cesium from contaminated areas, the adsorbent used would need to form strong bonds with cesium, not release toxic compounds, and be stable under heat

and radiation. One particular class of compounds fulfilling these characteristics is heteropolyacids.

Heteropolyacids

A heteropolyacid (HPA) is a class of acid containing a particular combination of certain metals, non-metals, oxygens and acidic hydrogens (Figure 1). The metal in the HPA is known as

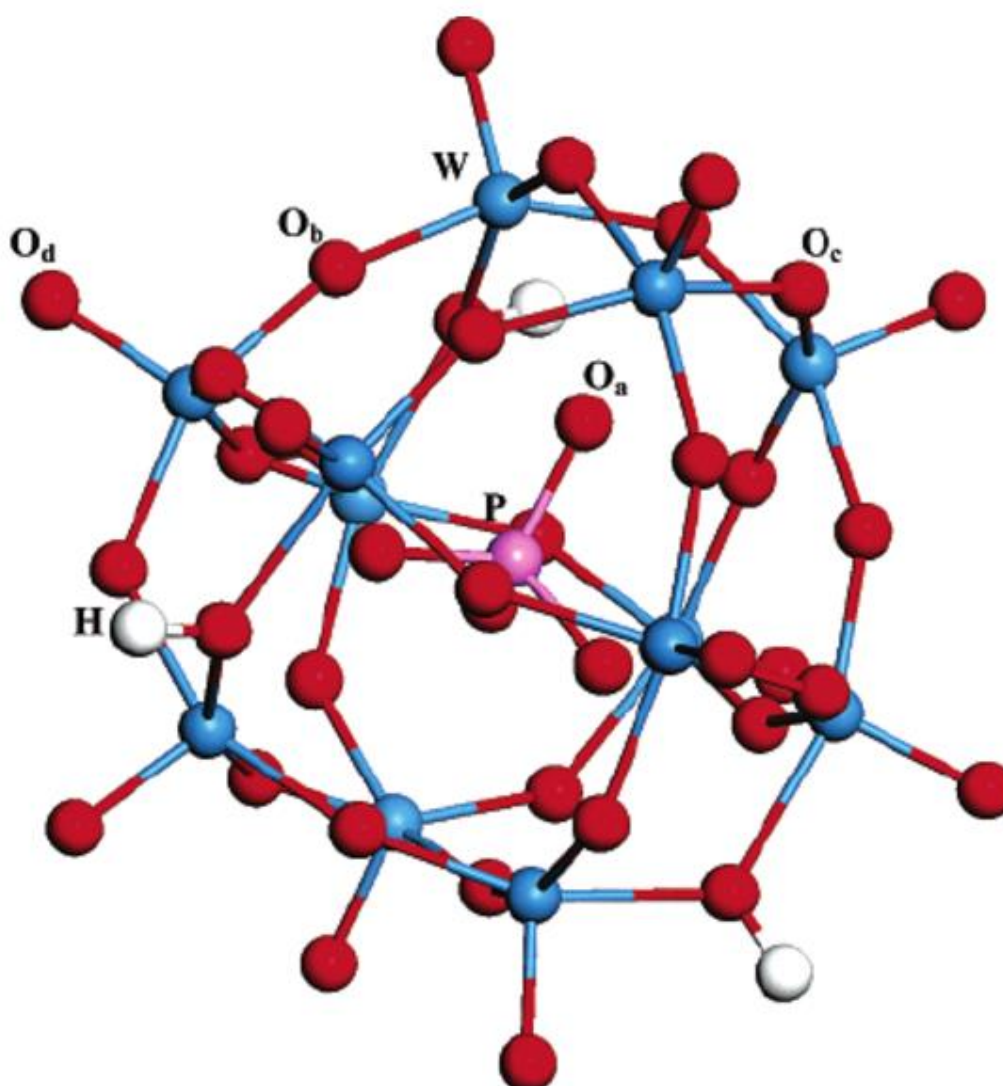


Figure 1: The Keggin structure of $\text{H}_3\text{PW}_{12}\text{O}_{40}$

the addenda atom, while the central atom (generally a p-block element such as silicon or phosphorus) is termed the hetero atom. The heteroatom is bonded to the rest of the structure via oxygen atoms, which are linked by the addenda atoms, and the hydrogens are bonded to either bridged or terminal oxygens. There are many different configurations of HPAs due to the large number of combinations of addenda and hetero atoms, but the focus in this work will be on the Keggin structure, $H_nXM_{12}O_{40}$, where X is the hetero atom and M is the metal

HPAs have become well known for their environmentally friendly nature as solid acids as well as their high catalytic activity. HPAs are considered superacids due to their very strong Brønsted acidity, being stronger than typical mineral acids such as H_2SO_4 or HNO_3 .^{18,19} For catalytic reactions, the catalytic properties of HPAs directly depend on their acidities. In order to understand the acidity and thus the catalytic activity of HPAs, the proton sites of the compound must be characterized. The Keggin HPA structure has three types of outer oxygen atoms that can possibly be protonated: two types of bridging oxygens (M – O – M), as well as terminal oxygens (M=O). Due to the increased electron density present on the bridged oxygens, these sites are protonated preferentially to terminal oxygens.¹⁸

Solid HPAs are acidic only by the Brønsted definition, and are stronger than typical solid acids such as silica, alumina and common zeolites. Acidities of typical solid HPAs of the Keggin type are in the order of PTA > SiTA > PMA > SiMA.^{19,20} PTA ($H_3PW_{12}O_{40}$) is a strong, fully dissociated acid in aqueous solution, with the anion remaining deprotonated after receiving two or even three additional electrons.²¹

Their acidity can be increased further by partial neutralization with different cations, such as Na^+ , K^+ and Cs^+ , with the solubility of the resulting salt decreasing in the order of $Na^+ > K^+ >$

Cs⁺.²² Interestingly, when acidic protons are exchanged with Cs⁺ in PTA, the acidity of the compound increases dramatically. This effect is most prominent when the number of Cs atoms per PTA molecule is 2.5 (Cs_{2.5}H_{0.5}PW₁₂O₄₀).²³

Due to the high stability of Cs⁺-HPAs and their selective formation in the presence of other alkali metals, these compounds possess great potential for applications in cesium removal. Preparing Cs⁺-HPAs simply consists of adding an aqueous Cs⁺ salt to an aqueous solution of the HPA with stirring, then drying the resulting material. The Cs content on the HPA can be adjusted by using different stoichiometric ratios of the Cs⁺ salt with respect to the HPA.²²

As a part of the successful development of an efficient adsorbent for cesium contamination, the acidity of surface sites should be well understood. There are different methods to analyze the acidity of solid materials, with the most common of these being temperature-programmed desorption and direct titration. The first option for determining the acidity of the material is temperature-programmed desorption of adsorbed bases such as ammonia or pyridine, which are used as probe molecules. In this method, the relative acidity of different sites is obtained from the temperature at which the probe molecule desorbs from the material's surface, with the bond strength of the acidic site and the probe molecule depending on the acidity of the individual site. Afterwards, the peak area can be integrated to determine the total number of acidic sites present on the surface of the material.²⁴ This method gives precise determination, but there are significant drawbacks to using this method. Temperature-programmed desorption requires very expensive equipment, runs only one sample at a time and each sample can take up to an entire day to analyze. Because of this, titration is the most convenient method for analyzing the surface acidity of multiple solid samples. In this case however, the solid material is unstable in alkaline media due to the presence of PTA in the

molecular framework. Consequently, traditional determination of acidity by direct titration is not feasible.

With this in mind, one of the main objectives of this work was to develop methodology for titration of a solid mesoporous material unstable in basic media to determine the number of surface acidic sites present in the material.

Incorporation of Heteropolyacids to Silica Gel

A wide array of chemical syntheses in industry utilize homogeneous acids and bases. These generally result in large volumes of hazardous waste being produced, which is coupled with high treatment and/or disposal costs. This presents a high demand for cleaner liquid phase chemical processes.²⁵ Molybdenum- and tungsten-containing HPAs have found many catalytic applications in oxidation, alkylation, esterification, and many other reactions in industry.²⁶ HPAs are insoluble in non-polar solvents, making them environmentally friendly and promising heterogeneous acid catalysts to replace potentially harmful homogeneous acid catalysts while preserving catalytic activity.^{26,27} However, their low surface area limits their application. HPAs have a high degree of Brønsted acidity, but low surface area limits efficiency due to a limited number of acid sites for catalytic reactions, and catalytic activity depends directly on the acidity of the material.²⁶⁻²⁸

With these properties in mind, HPAs, particularly the Keggin-type ($\text{H}_3\text{PW}_{12}\text{O}_{40}$), possess a wide array of potential environmental and economic benefits.²⁹ To increase applicability, it is necessary to disperse the HPA onto a support with large surface area. Non-basic substances such as activated carbon and ion-exchange resins are suitable, but SiO_2 is most often used due to its high surface area, regular geometry and being essentially inert towards HPAs. Two different

routes have been utilized in the bulk of the literature to immobilize HPAs (or polyoxometallates) onto porous support: impregnation and co-condensation using the sol-gel technique.²⁷⁻³⁰

Impregnation involves simply introducing the HPA to an already-formed silica structure. This technique is simpler but generally results in loss of homogeneity due to structure changes and difficulties in achieving high loading percentages.³⁰ In addition, due to the HPA being introduced to the surface and not incorporated into the silica structure, it is very soluble in polar solvents, thus resulting in a high degree of leaching. These combined attributes lead to low stability and activity of the HPAs, resulting in an undesirable material for use in aqueous media.³⁰

The other method of interest is a direct synthesis which utilizes co-condensation using the sol-gel method. The sol-gel process involves the formation of a *sol* and crosslinking to form a *gel*. These reactions are typically carried out using polar solvents such as ethanol, which is essential for the primary reactions that take place: *hydrolysis* and *condensation*. A step-wise polymerization occurs, causing a continual increase of molecular weight of the product, eventually forming a three-dimensional highly cross-linked network.^{30,31} This process often takes several days to complete, but the addition of an acid or base catalyst greatly speeds up the process and can also affect the physical properties of the product obtained. It should be noted, however, that although this process can be carried out in acidic or basic media, HPAs are very unstable in basic media. As a result, it is necessary to perform the synthesis in acidic conditions.³⁰

The reaction proceeds via S_N2 mechanism (Figure 2). In an acid-catalyzed system, the protonation of the oxygen on the alkoxy group causes electron density to be withdrawn from Si,

resulting in a nucleophilic attack from a water molecule and the loss of ethanol as a leaving group.

Proceeding the nucleophilic attack, the ethoxy group is replaced with a hydroxyl group, which allows condensation to occur between multiple molecules. The resulting material after polycondensation is a three-dimensional oxide network.³⁰

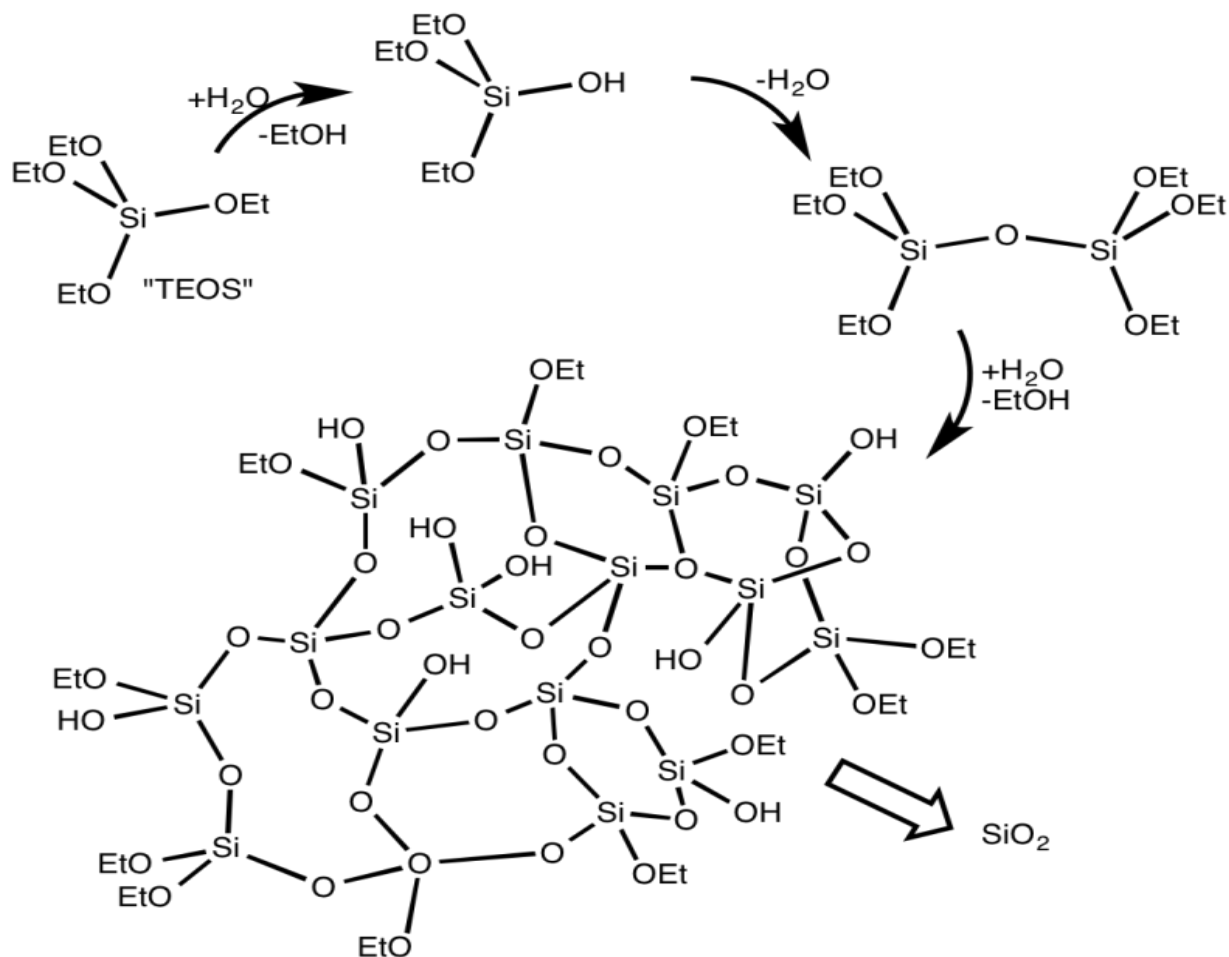
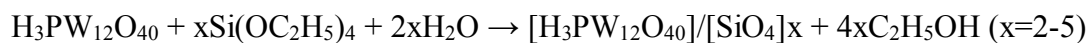


Figure 2: The acid-catalyzed polycondensation of TEOS

Introduction of HPAs into a silica network involves the co-incorporation of an oxide precursor with HPA clusters using the sol-gel technique. By doing this, HPAs are incorporated

into the framework of the material covalently by formation of W-O-Si bonds. This is shown by the following equation:



In addition, the presence of a surfactant during synthesis yields highly mesoporous materials, which is necessary when high surface areas are desired (Figure. 3).

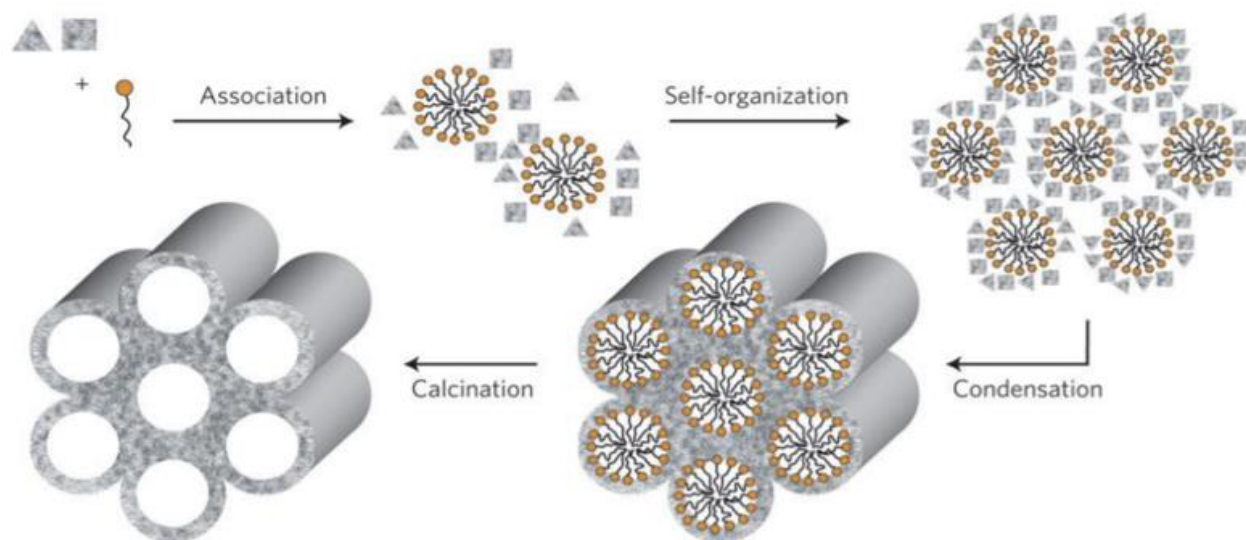


Figure 3: The formation of a porous system using a surfactant in sol-gel synthesis³²

The preparation of materials using a direct synthesis of this type yields materials with large pore sizes with a more stable and uniform distribution of active sites, thus enhancing the performance of the material, as successfully demonstrated by Li, *et al.*^{28,29} In addition, cross-link density, porosity and homogeneity can be controlled by using different solvent-removal methods and changing the type of catalyst used. Due to a higher control over the resulting product as well as the greatly increased stability of the HPA in the prepared material, the sol-gel technique is a much more advantageous method of preparation of porous silica materials.²⁹

With all of these techniques in mind, the use of phosphotungstic acid incorporated into a silica structure via sol-gel synthesis will be employed for effective cesium removal. Tungsten HPAs form strong bonds with cesium, so it may be potentially effective in selectively removing cesium from aqueous and biological environments. The overall goal of this research project is to develop a quantitative method of surface analysis of the adsorbents for accessible and inaccessible adsorption sites. First, the material to be used in the adsorption study will be synthesized by co-condensation of TEOS and tungsten containing HPAs. In this process, the metal oxides will be incorporated into the molecular framework. Surface hydrogens will be exchanged with cesium to study any differences in characteristics between the substituted and non-substituted material, then the contents of Cs and W will be determined by atomic absorption spectroscopy (AAS). The adsorbent will be characterized using FT-IR (Fourier Transform infrared spectroscopy), solid-state NMR (nuclear magnetic resonance), TEM (transmission electron microscopy) imaging, porosimetry, X-ray diffraction, and thermoanalysis. Batch adsorption tests, column tests and kinetic experiments will be done in order to understand the adsorption characteristics of the material. Finally, surface acidity and accessibility of adsorption sites will be quantified.

CHAPTER 2

EXPERIMENTAL / METHODOLOGY

Materials Used

Precursors for the adsorbent synthesis, tetraethoxysilane (TEOS) and phosphotungstic acid hydrate (PTA), were purchased from Acros Organics. (Morris Plains, NJ). Pluronic P123 with M.W.=5800, a pore-forming agent, was purchased from Sigma-Aldrich (St. Louis, MO).

Salts used in adsorption studies, $\text{CoCl}_2 \cdot 6\text{H}_2\text{O}$, $\text{SrCl}_2 \cdot 6\text{H}_2\text{O}$, KCl and NaCl were purchased from Fisher Scientific (Pittsburg, PA). HF (48%), used for the dissolution of silica, was purchased from VWR International, LLC. (Radnor, PA).

Bases used for acidity determination, pyridine and diphenylamine, were purchased from Acros Organics (Morris Plains, NJ.) and J.T. Baker Chemical Co. (Phillipsburg, NJ), respectively.

Common solvents used in this work include acetone, THF and ethanol. Other miscellaneous chemicals used were HCl, KBr, Na_2CO_3 and NH_4OH .

Synthetic Methods

The adsorbent H-PTA/ SiO_2 was synthesized using a slightly modified procedure published earlier.³³ Two solutions were prepared. Pluronic P123 (50 g) was dissolved in 150 mL of ethanol, and separately TEOS (72 g) and PTA (18 g) were dissolved in 50 mL of ethanol. Then solutions of TEOS/PTA and 20% HCl (150 mL) were added dropwise simultaneously to the solution of the surfactant under stirring. The reaction mixture was refluxed for 24 h. The

resulting gel was filtered, washed with deionized water until complete removal of the acid, then rinsed with acetone and air dried overnight. The sample was calcined at 500 °C for 5 h.

Cs-exchanged material Cs-PTA/SiO₂ was prepared by mixing 8.2 g of H-PTA/SiO₂ with 100 mL of 0.13 M solution of CsCl. The mixture was stirred overnight, washed by deionized water, and air dried overnight.

Instrumental Characterization

Elemental Analysis

Contents of Cs and W in the samples were determined through atomic absorption spectrometry (AAS) using a Shimadzu AA-6300 spectrometer (Kioto, Japan). The samples for measurement were prepared by dissolution of the materials in 48% HF (VWR International, Radnor, PA) followed by neutralization by NH₄OH to pH=7. Concentrations of Cs⁺, Sr²⁺ and Co²⁺ in solutions after adsorption were measured on the same instrument.

Chemical stability of adsorbed Cs in acidic and basic media was examined by the treatment of Cs-PTA/SiO₂ samples (0.1 g each) with 10 mL of 11.6 M HCl and 2.3 M Na₂CO₃ solutions for 2 h. Then the contents of leached Cs⁺ were analyzed by AAS.

Surface Acidity

Surface acidity of the samples was determined by reversed titration. Keggin units are unstable in aqueous media at high pH, thus the neutralization of acidic sites on the samples was conducted in anhydrous THF. The samples were dried overnight at 140°C to remove physically adsorbed water molecules. Then 0.1 g of each sample was dispersed in 6 mL of 0.01 M solution of pyridine or diphenylamine in dry THF. The mixture was allowed to equilibrate for 18 h at 23 °C. After equilibration, the solution was decanted from the solid, diluted by 100 mL of DI water

and titrated by 0.01 M HCl until pH=3. Obtained data were compared to the blank solution prepared without the solids. The data were recorded on an Orion 350 pH meter (Thermo Scientific, Pittsburg, PA). The volumes occupied by pyridine and diphenylamine molecules were calculated using Spartan software and found to be 93 and 196 Å³, respectively.

Spectral Analysis

FT-IR spectra were recorded in KBr pellets on a Vertex 70/80 FT-IR spectrometer (Bruker Optics, Inc., Billerica, MA).

All solid state NMR spectra were acquired on a Bruker AVANCE 400 spectrometer (Rheinstetten, Germany). ²⁹Si spectra were recorded at 79.49 MHz, pulse length: 6 μs, delay time: 15 s, number of scans: 50,000. Relative intensities of the signals were calculated by deconvolution of the spectra using the Gaussian function on Origin 2016 software. ¹H NMR spectra were recorded at 400.13 MHz, pulse length: 12 μs, delay time: 2 s. The number of scans was 128. Chemical shifts were referenced to external TMS. For recording ³¹P spectra, the experiments were conducted at 162 MHz, pulse length: 14 μs, delay time: 10 s, number of scans: 1024. Chemical shift was measured in respect to 85% H₃PO₄. ¹³³Cs spectrum was recorded at 52.48 MHz, pulse length: 12 μs, delay time: 0.5 s, number of scans: 1024. The standard was CsCl solution in D₂O. Before measurements, samples were dried at room temperature in a vacuum until the weight was constant.

Structure and Morphology

Transmission electron microscopy (TEM) images were obtained on a JEOL 1230 electron microscope (Tokyo, Japan) at 80 kV. Before imaging, samples were dispersed in a 50% ethanol solution using a W-385 sonicator (Heat Systems Ultrasonic, Newtown, CT) for 2 min.

Porous characteristics were measured on a Quantachrome Nova 2200e porosimeter (Boynton Beach, FL). Prior to measurements, the samples were degassed at 300 °C in vacuum for 2 h. The Brunauer–Emmett–Teller (BET) surface areas were calculated from the adsorption branch of isotherms in the range $P/P_0=0.2-0.4$. Pore size distributions were obtained using *Density Functional Theory* (DFT) method. Micropore volumes were calculated by *Saito–Foley* (SF) method. All calculations were performed using NovaWin v.11.02 software.

Particle sizes were determined by dynamic light scattering on a Zetasizer Nano ZS90 (Malvern, UK). The samples were dispersed in water at sonication.

X-ray diffraction (XRD) patterns were recorded on a Dron 2.0 diffractometer (St. Petersburg, Russia) using an X-ray tube with a copper anode and a nickel filter at 30 kV and 15 mA. The patterns were collected in the range of angles 2θ from 5 to 40° that corresponds to a wave vector (q) values 3.6-27.9 nm⁻¹. The size of the corresponding domain was estimated using the Scherrer equation:

$$D=K\lambda/(\beta\cos\theta) \quad (1)$$

where D is the mean size of the ordered domains, K is a proportionality constant with a typical value of 0.9, λ is the X-ray wavelength (0.154 nm), β is the line broadening at half-height (taking into account instrumental broadening) (rad), θ is the Bragg angle (degrees).

Thermal Analysis

Differential scanning calorimetry (DSC) and thermogravimetric analysis (TGA) were provided by Robertson Microlit Lab. (Ledgewood, NJ). DSC analysis was conducted on a Pyris Diamond differential scanning calorimeter (Perkin Elmer, Waltham, MS) in a sealed pan. TGA analysis was conducted on a Perkin Elmer TGA 7 analyzer. The heat rate was 10 °C/min.

Adsorption

Batch Tests

Adsorption isotherms were constructed using data from the adsorption of Cs⁺ on H-PTA/SiO₂ at 23, 31 and 39 °C. Portions of the adsorbent (0.1 g) were dispersed in 10 mL of CsCl solutions with Cs⁺ contents of 100, 200, 300, 400 and 500 mg/L. The mixture was incubated for 2 h at constant temperature in a circulating water bath (Thermo Scientific, Pittsburg, PA). Then, the remaining concentrations of Cs⁺ in the solutions were measured using AAS. The equilibrium adsorption of Cs⁺ (q_e, mg/g) was calculated from the difference between the initial and the equilibrium (C_e, mg/L) concentrations.

The adsorption of Sr²⁺ and Co²⁺ was studied as described above using SrCl₂ and CoCl₂ solutions. In the selectivity study with Na⁺ and K⁺, equimolar amounts of NaCl or KCl were added to the CsCl solutions and the mixtures were processed at 23 °C as described above.

Fitting of the linearized form of adsorption isotherm equations to the experimental data was performed. For this purpose, the following three isotherm models were used:

1) Langmuir model:

$$1/q_e = 1/q_m + 1/q_m K_L C_e \quad (2)$$

2) Freundlich model:

$$\text{Log}q_e = \text{log}K_F + \text{log}C_e/n \quad (3)$$

3) Temkin model:

$$q_e = RT \ln(A_T C_e) / b_T \quad (4)$$

where K_L is the Langmuir constant (L/mg) related to the energy of adsorption, q_e and q_m are the metal ion concentration on the adsorbent at equilibrium and the maximum of monolayer adsorption capacity (mg/g), respectively, C_e is the equilibrium concentration of the metal in the solution (mg/L), K_F is the Freundlich constant (mg/g) related to the adsorption capacity, n is adsorption intensity, A_T is the equilibrium binding constant (L/g), b_T is the Temkin isotherm constant, R is the universal gas constant, 8.314 J/(mol•K), and T is the temperature (K).

Kinetic Studies

The process by which Cs^+ ions were removed from the solution by the adsorbent was explained using intraparticle and kinetic modeling, which examines the diffusion-controlled and rate-controlled mechanism of adsorption, respectively. Information on the diffusion of Cs^+ was obtained by plotting the adsorption of cesium vs. $t^{0.5}$ for five initial Cs^+ concentrations ranging from 100-500 mg/L. The intraparticle diffusion rates were calculated using the Weber-Morris equation:

$$q_t = k_{id}t^{0.5} + C \quad (5)$$

where q_t is the amount of Cs^+ (mg/g) adsorbed at time t (min), k_{id} is the rate constant of intraparticle diffusion (mg/(g•min^{0.5})), and C is the intercept (mg/g) related to the boundary layer thickness. The data were obtained as described above, with the exception that the solution samples were collected after 5, 10, 20, 40, and 60 min.

The linear form of the pseudo-first order equation:

$$1/q_t = k_1/q_e t + 1/q_e \quad (6)$$

as well as the pseudo-second-order equation:

$$t/q_t = 1/k_2 q_e^2 + t/q_e \quad (7)$$

were used to determine rate constants for the adsorption process, where q_t and q_e are the amounts of Cs^+ adsorbed at time t and at equilibrium (mg/g), respectively, k_1 and k_2 are the rate constants for pseudo-first order adsorption (min^{-1}) and pseudo-second-order adsorption ($\text{g}/(\text{mg}\cdot\text{min})$), respectively. Graphs were obtained for the pseudo-first-order model by plotting $1/q_t$ vs. $1/t$, while plots of t/q_t vs. t were used to obtain graphs for the pseudo-second-order model.

Column Tests

Column tests were conducted using CsCl solutions of 100, 200, 300, 400 and 500 mg/L concentrations. The solutions passed through a column containing 0.1 g of H-PTA/SiO₂ mixed with sand as a filler with a flow rate of 1.5 mL/min. Filtrate samples were collected every 2 mL and analyzed by AAS.

CHAPTER 3

RESULTS AND DISCUSSION

Synthesis and Composition

Gelation of the solution started about 1 h after the start of reflux. Yield of the product was 37.3 g, corresponding to a 96% conversion of TEOS and PTA to the product. Content of PTA in the obtained material was determined from analysis of tungsten (Table 1) using AAS and was found to be 18.4% (0.064 mmol/g). After Cs exchange, the material was found to contain 17.1% of PTA (0.059 mmol/g) and 2% of Cs (0.15 mmol/g). Thus the molar ratio Cs/PTA after adsorption was 2.54.

Cs-PTA/SiO₂ was relatively stable in acidic and basic media. The leaching of Cs⁺ in HCl solution was 4.6 mg/g while in Na₂CO₃ solution it was only 3.5 mg/g. A more alkaline solution was not used due to the low stability of the silica network at high pH media.

Table 1: Characteristics of H-PTA/SiO₂ and Cs-PTA/SiO₂

Characteristic	H-PTA/SiO ₂	Cs-PTA/SiO ₂
Contents of W, mg/g	141	131
Contents of Cs, mg/g	-	20.2
Acidity (pyridine), mmol/g	0.12	0.15
Acidity (diphenylamine), mmol/g	0.09	0.19
BET surface area, m ² /g	582	597
Total pore volume, cm ³ /g	0.49	0.44
Micropore volume, cm ³ /g	0.17	0.18
Average pore diameter, nm	4.89	4.89
Average micropore diameter, nm	0.35	0.45
Average particle size, nm	520	589
Polydispersity index	0.46	0.51

Instrumental Characterization

FT-IR Spectroscopy

FT-IR spectra of H-PTA/SiO₂ and Cs-PTA/SiO₂ (Figure 4) have characteristic bands of silica gel at 470, 810, 1080, 1650 and 3480 cm⁻¹. In addition, they have peaks assigned to the

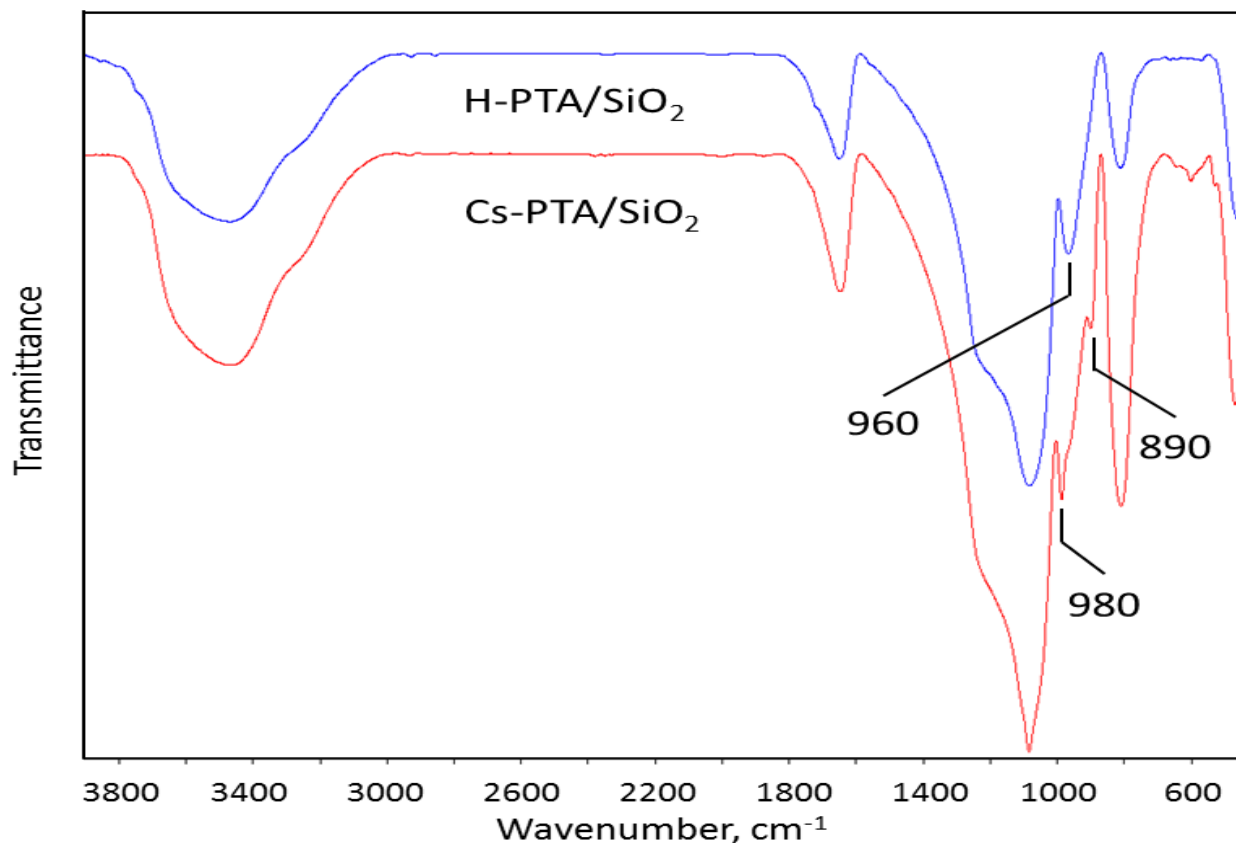


Figure 4: FT-IR spectra of H-PTA/SiO₂ and Cs-PTA/SiO₂

Keggin structure of PTA. In the spectrum of H-PTA/SiO₂ one broad band is located at 960 cm⁻¹. The same band in the spectrum of Cs-PTA/SiO₂ contains two sharp peaks at 980 and 890 cm⁻¹ ($\nu_{W=O}$ terminal and ν_{W-O-W} corner, respectively).³⁴ Treatment by CsCl solution produced changes in the chemistry and structural characteristics of H-PTA/SiO₂. The acidic form of the adsorbent contains protonated bridged W-O-W and terminal W=O groups in the Keggin structure.

Protonation and, as a result, presence of hydrogen bonds causes broadening of corresponding peaks at 980 and 890 cm^{-1} in the FT-IR spectra that makes them undetectable. In contrast, the spectrum of Cs-PTA/SiO₂ has narrow peaks at these wavelengths.³⁵

Solid State NMR Spectroscopy

Solid state NMR spectra of ¹H, ²⁹Si, ³¹P and ¹³³Cs are presented in Figure 5. ²⁹Si NMR spectra of both materials contain four major signals at -75, -82, -103, and -108 ppm. The last three signals are present in typical spectra of amorphous silica gel and correspond to (Si-O)₂Si(OH)₂ (Q²), (Si-O)₃Si-OH (Q³), and (Si-O)₄Si (Q⁴) silicon atoms, respectively. The first downfield signal not observed in the silica spectra might be attributed to silicon atoms bonded to tungsten of Keggin units (Si-O)₃Si-O-W.³⁶ High intensity of this signal shows that a significant fraction of Si atoms are bonded covalently to W atoms via oxygen bridges.

For H-PTA/SiO₂, the ratio of the signal intensities was found to be 0.36:0.18:0.09:0.37. Thus most silicon atoms did not contain silanol groups. After the adsorption of Cs⁺ cations, this ratio changed to 0.38:0.29:0.23:0.10. Relative contents of Q² and Q³ Si atoms increased notably for the account of Q⁴ atoms. The number of Si-O-W bridges did not change significantly. It is clear that in the solution of CsCl, hydrolysis of Si-O-Si bridges occurs. This process might be catalyzed by free acid released during exchange of protons by Cs⁺ cations after adsorption.³⁷ Change in acidity of the sample after ion exchange with Cs was clearly evident from solid state ¹H NMR spectra. The signal of protons shifted from 7.49 to 2.43 ppm. It is known that PTA is a superacid and the signal of protons in NMR spectra are located at 9 ppm. In the partially exchanged Cs⁺ salt, another signal at 5 ppm appears.³⁸ The first signal can be attributed to superacidic OH groups, which are H-bonded to adjacent Keggin anions. The second signal represents less acidic OH groups without H-bonds. Pure silica gel contains peaks in the region of

1.7-3.5 ppm. Due to the broadening effect in solid state, the spectra of H-PTA/SiO₂ and Cs-PTA/SiO₂ contain only one broad peak. However, the position of this peak enabled the estimation of relative contributions of different acidic sites in the samples. The signal at 7.49 ppm (H-PTA/SiO₂) indicated the presence of superacidic sites while the peak at 2.43 ppm showed a lower contribution of strong acidic sites in the acidity of Cs-PTA/SiO₂.

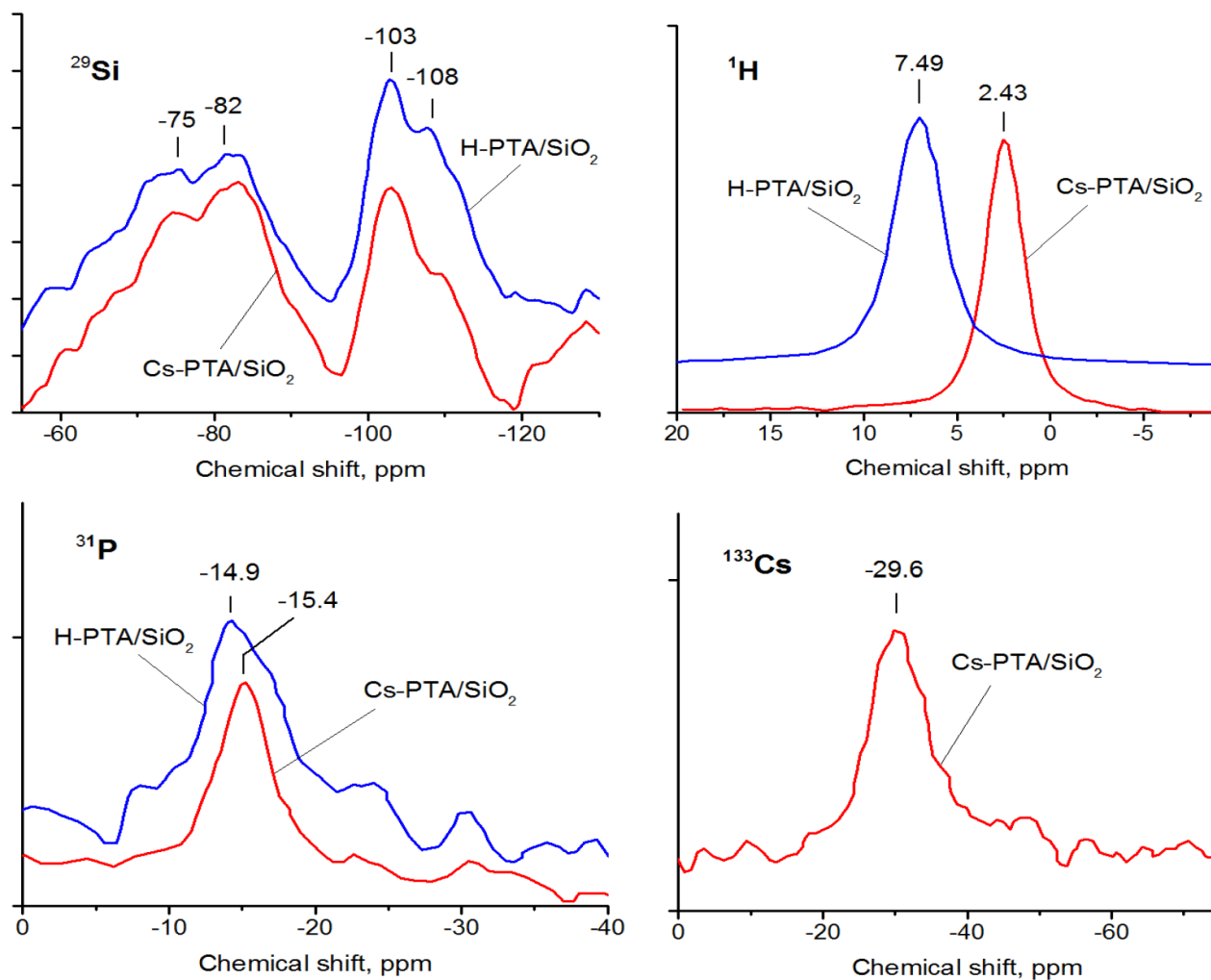


Figure 5: Solid state NMR spectra of H-PTA/SiO₂ and Cs-PTA/SiO₂

Anhydrous PTA has one peak at -10.9 ppm in the ³¹P NMR spectrum. This signal was attributed to protons directly bonded to bridging oxygens of Keggin anions. For hexahydrated

PTA, this signal is shifted to -15.6 ppm, which is very close to the data reported in literature for supported PTA (-15.0 ppm) and our experimental data (-14.9 ppm).³⁹ Thus acidity of H-PTA/SiO₂ is produced by protonated water molecules bonded to the terminal oxygens of PTA via H-bonds. Position of the signal of Cs-PTA/SiO₂ (-15.4 ppm) is also very similar to literature data.⁴⁰ Little upfield shift after ion exchange might be caused by shielding effect of the electron-rich anion of the Keggin structure. Presence of only one signal proved that no partially Cs-exchanged PTA molecules were present in the sample.

The presence of Cs⁺ in the exchanged adsorbent was confirmed by ¹³³Cs solid state NMR. In the spectrum of Cs-PTA/SiO₂, a signal at -29.6 ppm is located in the region typical for hydrated Cs⁺ cations adsorbed on clay materials. Chemical shift of ¹³³Cs depends on its coordination number: electrons of oxygen atoms coordinated to Cs⁺ provide a shielding effect. Earlier it was suggested that the signal at this position can be attributed to 9-coordinated Cs⁺ cations.⁴¹

Surface Acidity

In order to determine the acidity and number of acidic sites of the adsorbent surface, direct titration was the method initially used. It was observed that the amount of OH⁻ absorbed was completely unrealistic, taking more than ten times the expected stoichiometric amount without reaching equilibrium. Because of this, a new approach needed to be developed. In the case of this material, acidic sites are adsorption sites, so in order to study adsorption, the acidity needs to be well characterized. In this work, a new analytical method was developed to study the acidity of solid porous materials unstable in basic conditions: reverse titration using organic bases in non-aqueous media.

Organic bases in dry THF were used for neutralization of acidic sites on the surface of the adsorbent. After neutralization, the remaining amount of unreacted base was titrated with HCl to determine the number of accessible surface acidic sites present. Experimental data obtained by titration with pyridine and diphenylamine are in agreement with theoretically expected acidity calculated from tungsten contents (0.19 mmol/g). Lower experimental values were caused by inaccessibility of a part of acidic sites located inside the silica network. Only acidic sites on the pore surface can interact with molecules of organic bases. These data also correlate with the relative sizes of organic base molecules. Titration curves for the titrations for both pyridine and diphenylamine are presented below (Figure 6).

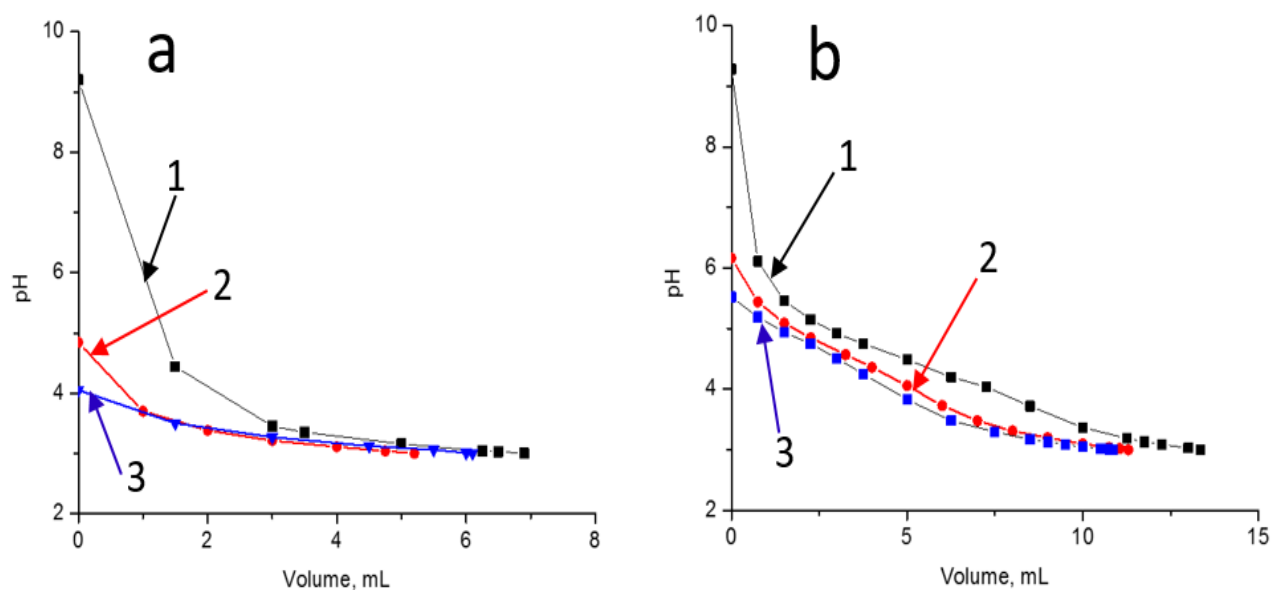


Figure 6: Titration curves for blank solution (1), 0.1 g Cs-PTA/SiO₂ (2) and 0.1 g H-PTA/SiO₂ (3) with pyridine (a) and diphenylamine (b)

Unexpectedly, after the substitution of most protons by cesium, the acidity of the samples increased. This effect was reported earlier for bulk PTA and its cesium salts of different compositions. In accordance with Dias *et al.*, the adsorption of pyridine on Cs_{2.5}H_{0.5}PW₁₂O₄₀ was

much higher than on $\text{H}_3\text{PW}_{12}\text{O}_{40}$.⁴² As calculated from the data in Table 1, the ratio Cs/W in Cs-PTA/SiO₂ corresponded to the most acidic reported material (2.5). The authors attribute this phenomenon to the increase of porosity and surface area of PTA at proton substitution. In addition, hydration of Keggin units can create additional acidic sites. In accordance with Okuhara *et al.*, one hydrated PTA anion can adsorb up to 8.5 molecules of pyridine.⁴³

TEM Imaging

The H-PTA/SiO₂ material was present in the form of small particles, mostly 200-500 nm. The presence of PTA was easily visualized due to phase contrast properties of tungsten in an electron beam.⁴⁴ PTA formed small spherical nanoparticles of 6-25 nm diameters. The product after exchange with Cs⁺ contained a significant amount of larger particles up to 1 μm . The samples had a disordered porous structure with pores about 5-8 nm diameter (Figure 7). Dark spots in the images of Cs-PTA/SiO₂ particles with sizes in the range of 6-25 nm are most likely Cs-exchanged PTA.

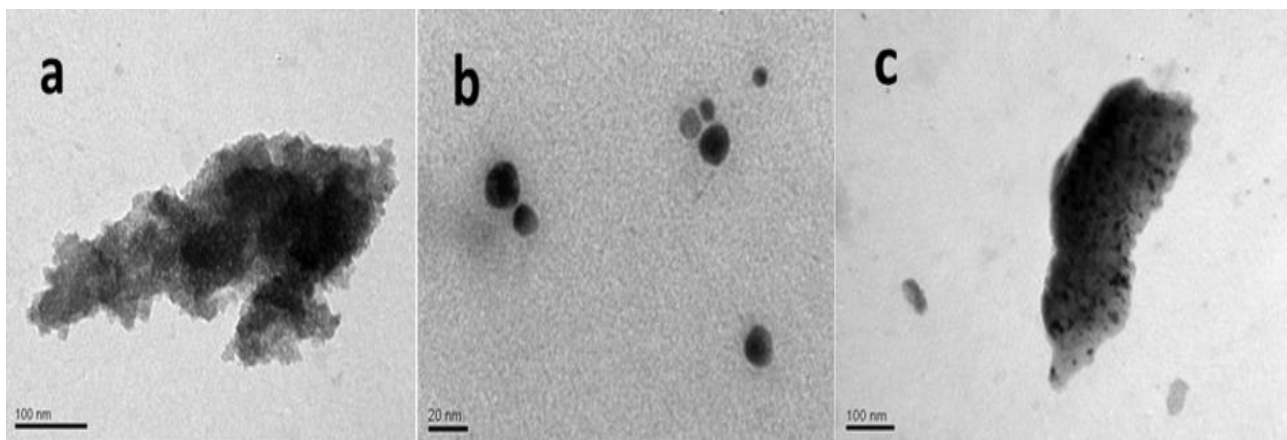


Figure 7: TEM images of H-PTA/SiO₂ (a and b) and Cs-PTA/SiO₂ (c)

Porosity

The obtained material was mesoporous but contained significant fraction of micropores in its structure. Adsorption/desorption isotherms belong to the type IV with H1 type of hysteresis loop, which is typical for cylindrical pores (Figure 8). The shape of desorption branch shows the presence of necks in the porous system.

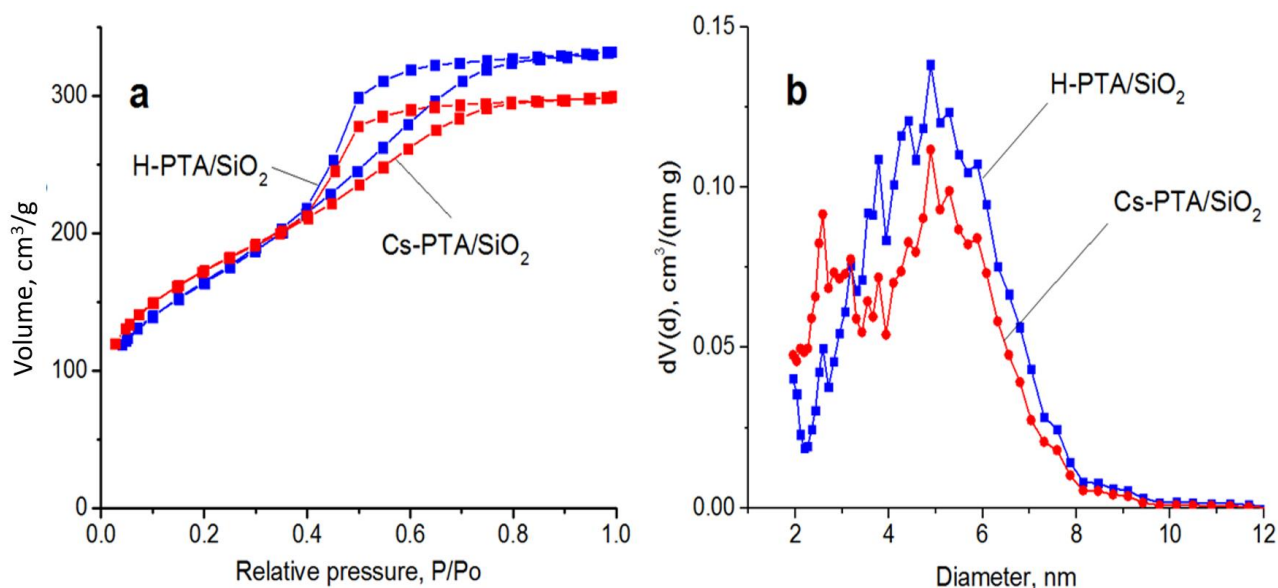


Figure 8: Nitrogen adsorption isotherms (a) and pore size distribution (b) of H-PTA/SiO₂ and Cs-PTA/SiO₂

The total pore volume of H-PTA/SiO₂ decreased after the adsorption of Cs⁺ (Table 1). This effect is expected as Cs⁺ ions occupy a much higher volume than protons. In addition, they may block access to small pores thus reducing accessible surface area. The adsorption of Cs⁺ did not change the average pore size but, surprisingly, the volume and average size of micropores somewhat increased. BET surface area of Cs-PTA/SiO₂ also somewhat increased.

The combination of reduced pore volume with increased BET surface area after ion exchange with Cs⁺ looks unusual. However, the formation of porous structures in non-porous

PTA after reaction with Cs_2CO_3 was reported and discussed in earlier works.⁴⁵ In particular, the authors noted that micropores provided the main contribution to the surface area. In Cs-PTA/ SiO_2 , the volume ratio of micropores to mesopores increased in respect to H-PTA/ SiO_2 .

Considering the known content of Cs in Cs-PTA/ SiO_2 and its BET surface area, the surface density of adsorbed Cs^+ was found to be 0.15 atoms/nm^2 .

Particle Size

Particles of H-PTA/ SiO_2 have diameters between 200 and 600 nm with the maximum at 342 nm. In the case of Cs-PTA/ SiO_2 , two groups of particles are present. Small particles 100-300 nm contribute 11.3% of total amount while larger ones (most likely agglomerates) have sizes in the range of 300-1100 nm with the maximum at 712 nm (Figure 9). The polydispersity index

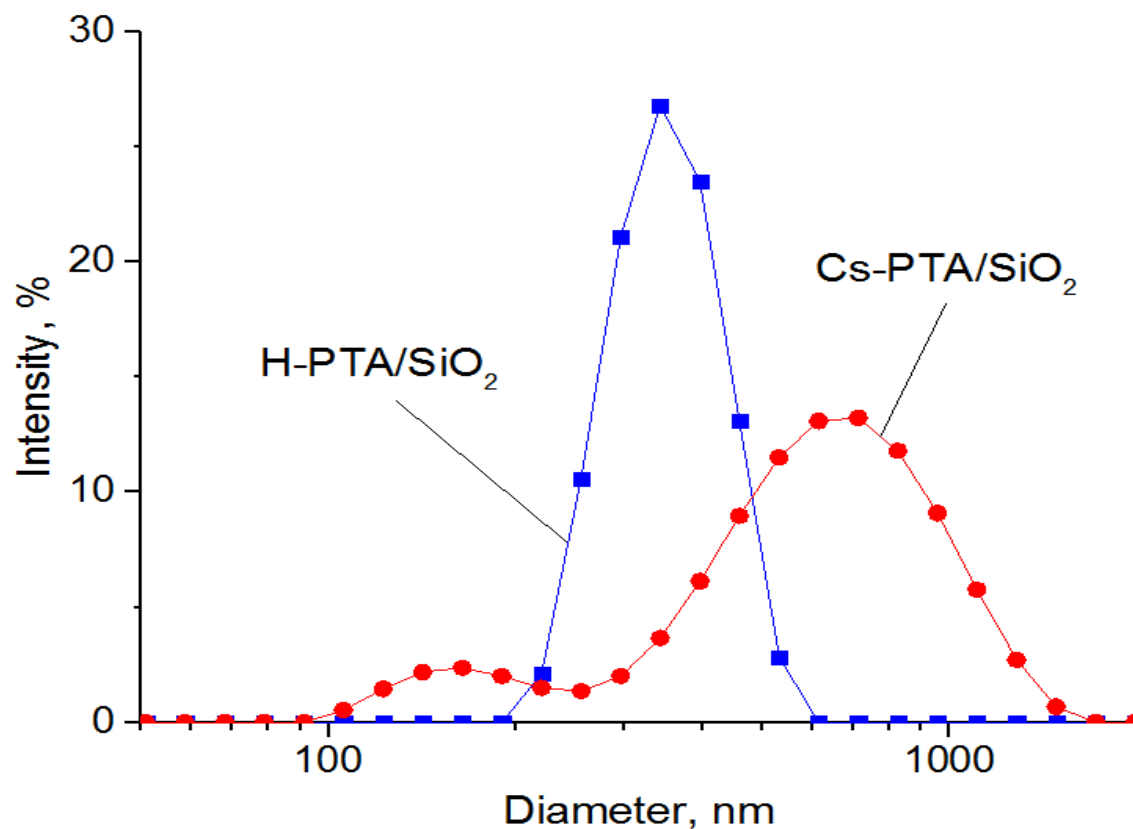


Figure 9: Particle size distribution of H-PTA/ SiO_2 and Cs-PTA/ SiO_2

increased after treatment with CsCl solution (Table 1).

It was evident that the treatment by the solution of CsCl caused strong agglomeration of the particles. This interesting effect was the result of high ionic strength of the solution. The surface of the particles had negative charge that resulted in the formation of protective double-layer. In the solutions with low ionic strength (e.g., deionized water), this double-layer extends beyond the range of the van der Waals force. Thus the electrical repulsion between particles prevented agglomeration. Higher ionic strength (e.g., solution of CsCl) reduced the size of double layer making the attractive van der Waals force stronger.⁴⁶

X-Ray Diffraction

The phase composition of the samples was clarified by XRD technique. XRD patterns showed an amorphous structure of the materials (Figure 10). The spectra showed a maximum in the broad peak at $2\theta=24.6^\circ$, which corresponds to *d*-spacing (average size of repeating units) of 0.34 nm.

It is known that the acidic form of PTA has XRD patterns of low intensity. Its Cs salt contains a much more intensive peak at $2\theta=26.4^\circ$.³⁴ The Cs-PTA/SiO₂ sample also had a small broad peak at $2\theta=24.2^\circ$ that might be attributed to immobilized Cs-PTA. Thus appearance of this peak at $2\theta=26.4^\circ$ after treatment by CsCl proved ion exchange in the adsorbent.

The size of a unit cell of a single Keggin unit is 2 nm.⁴⁷ The size of corresponding domains of Cs-PTA crystallites was found to be 11.8 nm, which is consistent with TEM data. Considering this value, it is evident that PTA was embedded in the silica matrix on the sub-molecular level.

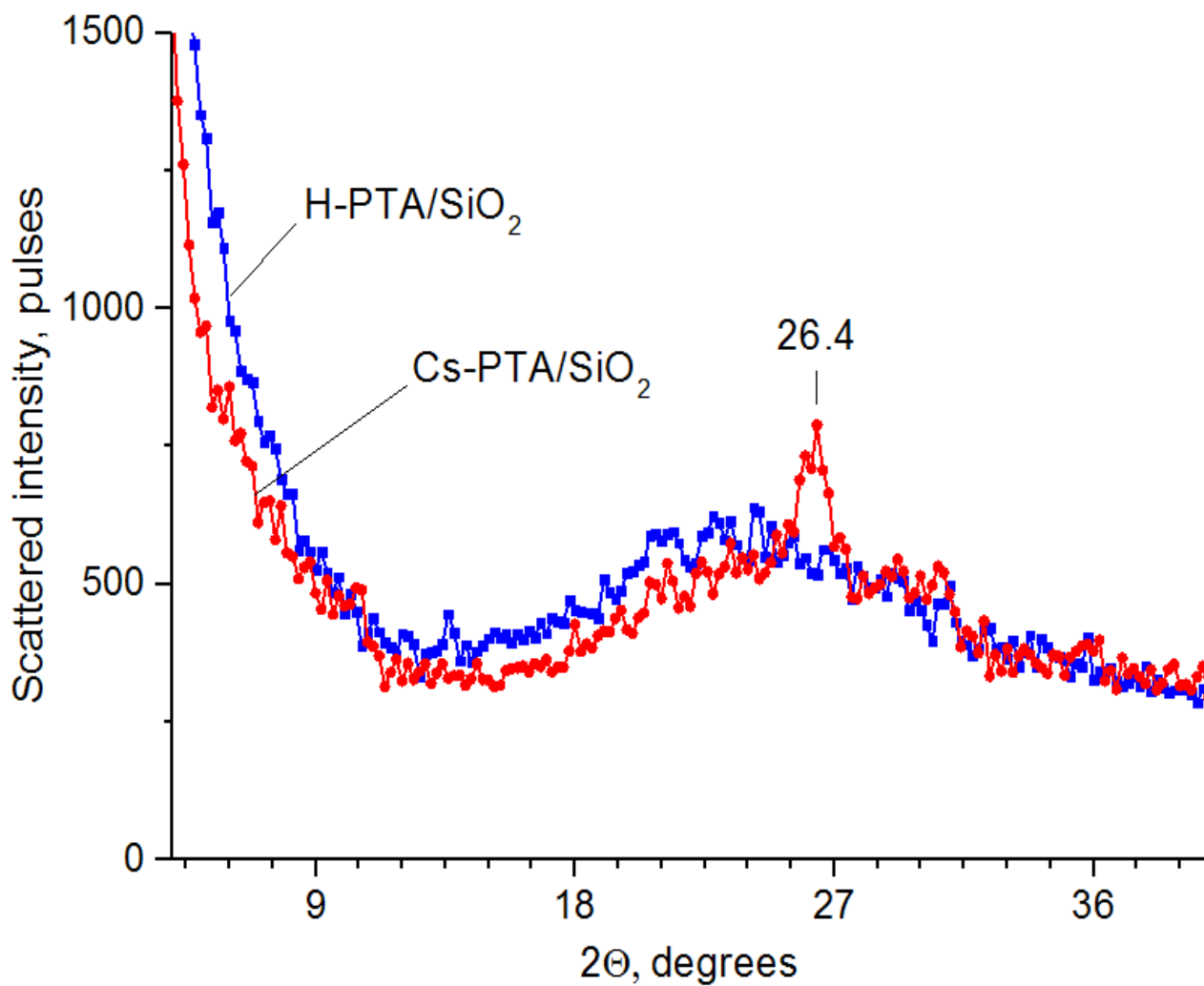


Figure 10: XRD patterns of H-PTA/SiO₂ and Cs-PTA/SiO₂

Thermoanalysis

The TGA curve of H-PTA/SiO₂ (Figure 11) shows a sharp loss of mass before 100 °C, which can be attributed to the evaporation of physically adsorbed water. In this temperature range, the material lost 8% of its total weight. At temperatures above 100 °C, the weight loss with temperature became gradual. The sample lost 4% more between 100 and 700 °C, which

proved a constant dehydration of the sample. It was not possible to distinguish between dehydration of silica or PTA phases as they occur simultaneously.

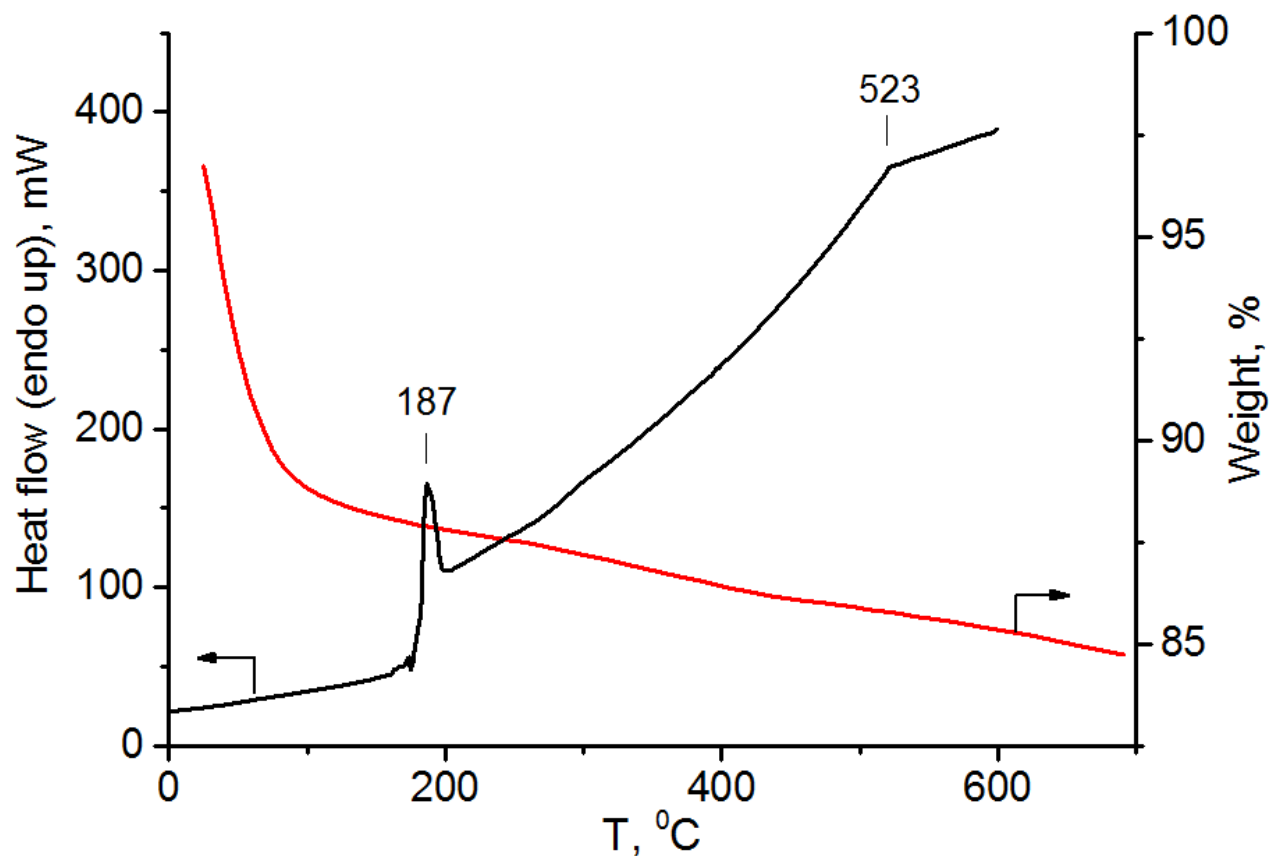


Figure 11: DSC and TGA curves of H-PTA/SiO₂

The phase change in H-PTA/SiO₂ at heating was detected by DSC analysis. In the DSC thermogram, an endothermic peak with the enthalpy $\Delta H=572$ J/g was observed at 187 °C. A similar event was reported earlier for pure PTA.⁴⁸ It corresponds to the lattice dropping from 12.17 to 11.78 Å although it still remained cubic. After this event, the baseline shifted to the endothermic side up to 523 °C where the shift became more gradual. The change of slope at 523 °C might be attributed to complete loss of constitutional water (acidic protons).³⁵

Adsorption Studies

Adsorption of Cesium

At temperatures below 31 °C, the adsorbent almost completely removed Cs⁺ from solutions when its concentrations did not exceed 200 mg/L (Figure 12a). It also demonstrated

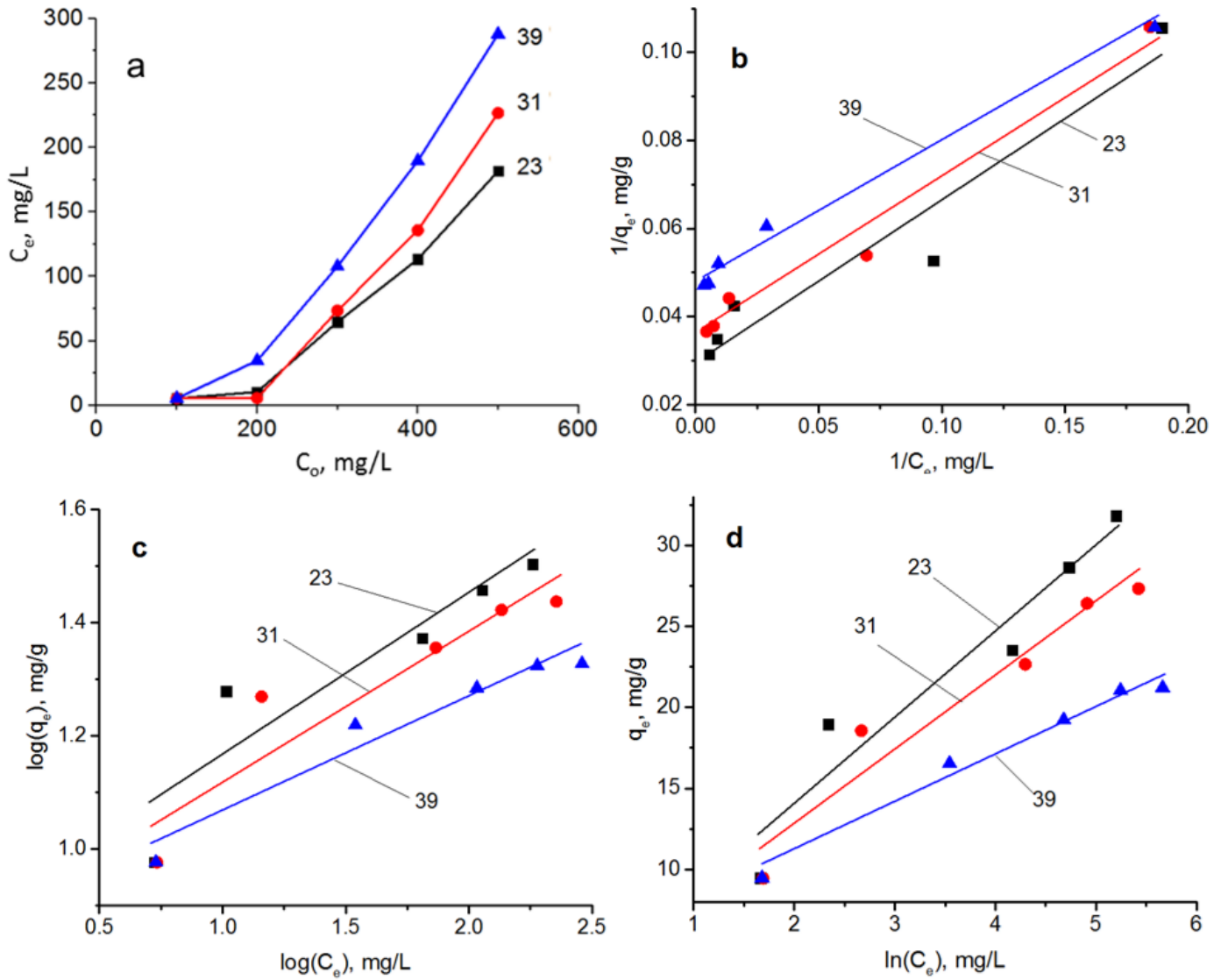


Figure 12: Adsorption of Cs⁺ by H-PTA/SiO₂ (a) and linear fitting plots of Langmuir (b), Freundlich (c) and Temkin (d) isotherm models at 23, 31 and 39 °C

high removal effectiveness at higher concentrations. Adsorption capacity at the equilibrium point depended on temperature. In the solution with concentration 500 mg/L, this characteristic decreased from 31.9 to 21.2 mg/g when the temperature increased from 23 to 39 °C.

Graphs of the obtained adsorption data applied to the linearized Langmuir, Freundlich and Temkin models are shown in Figures 12b-d, along with the degree of water purification at various temperatures (Figure 12a). The parameters of the models are shown in Table 2. From the correlation coefficients (R^2) obtained for the three models, the adsorption data are fitted to the Langmuir and Temkin models reasonably well.

It can be found from the correlation coefficients presented in Table 2 that the adsorption data were better fitted at higher temperatures. This can be attributed to the various types of adsorption occurring at different temperatures. At room temperature, two types of adsorption occur in general. The Cs^+ ion can be adsorbed via ion exchange onto the heteropolyacid surface as well as surface silanol groups. The $W-O^-Cs^+$ ionic bond is much more stable than $Si-O^-Cs^+$. With an increase in temperature, Cs^+ ions were displaced by H^+ on the silanol groups, while the PTA-adsorbed Cs^+ remained immobilized.

Table 2: Parameters of Adsorption

T, °C	Langmuir			Freundlich			Temkin			
	q_m , mg/g	K_L , L/mg	R^2	K_F , L/g	$1/n$	R^2	A_T , L/g	b_T	B , J/mol	R^2
23	33.0	0.083	0.966	7.275	0.290	0.928	1.612	448.56	5.4891	0.964
31	28.7	0.094	0.990	7.344	0.258	0.933	2.347	563.10	4.4907	0.966
39	20.8	0.150	0.995	7.163	0.205	0.974	5.174	861.17	3.0136	0.990

With this increase in temperature, the models have a better fit because the type of adsorption being studied is representative of PTA binding sites instead of a mixture of different types of adsorption.

This is further supported by the different equilibrium binding constants observed at various temperatures. The strength of the adsorption (A_T) increases with temperature (Table 2). At the lower temperature, it is lower due to the presence of Cs^+ adsorption onto Si-OH groups, which is less stable as compared to the strong interactions of Cs^+ with W=O groups of the Keggin structure. At higher temperatures, the binding constant is more representative of the interaction of Cs^+ with the heteropolyacid.

This was also observed for calculated values of B (J/mol) obtained from the Temkin isotherm, which is related to the heat of adsorption:

$$B = RT/b_t \quad (8)$$

At higher temperatures, the A_t and B values are more representative of the interaction of Cs^+ with the heteropolyacid.

The q_m values for adsorption capacity calculated by the Langmuir model (Table 2) indicate a high adsorption capacity towards Cs^+ . Discrepancy of adsorption capacity at different temperatures is due to the absence of adsorption onto silanol groups at higher temperatures. Thus, the adsorption capacity corresponding to ion-exchange on the PTA surface of the adsorbent was found to be 20.83 mg/g. The Langmuir model assumes a homogeneous monolayer adsorption process, while the Freundlich model assumes heterogeneous adsorption. Due to the much stronger agreement of the data with the Langmuir model, the adsorption process is homogeneous and depends on the active sites of the adsorbent surface.⁴⁹

Selectivity

In the experiments with NaCl and KCl, an effect of competing ions was evident. However, the adsorbent maintained good characteristics in the selective adsorption of Cs^+ (Figure 13). While the effect of sodium ions was negligible (decrease of adsorption capacity at 500 mg/L from 31.9 to 28.2 mg/g), potassium affected adsorption of Cs^+ somewhat stronger and reduced it down to 22.6 mg/g. This result correlates with relative solubilities of corresponding phosphotungstates: $\text{Na}_3[\text{PW}_{12}\text{O}_{40}]$ is very soluble, the solubility of $\text{K}_3[\text{PW}_{12}\text{O}_{40}]$ is much lower (about 1 mmol/L), while $\text{Cs}_3[\text{PW}_{12}\text{O}_{40}]$ is practically insoluble (3.4×10^{-3} mmol/L).

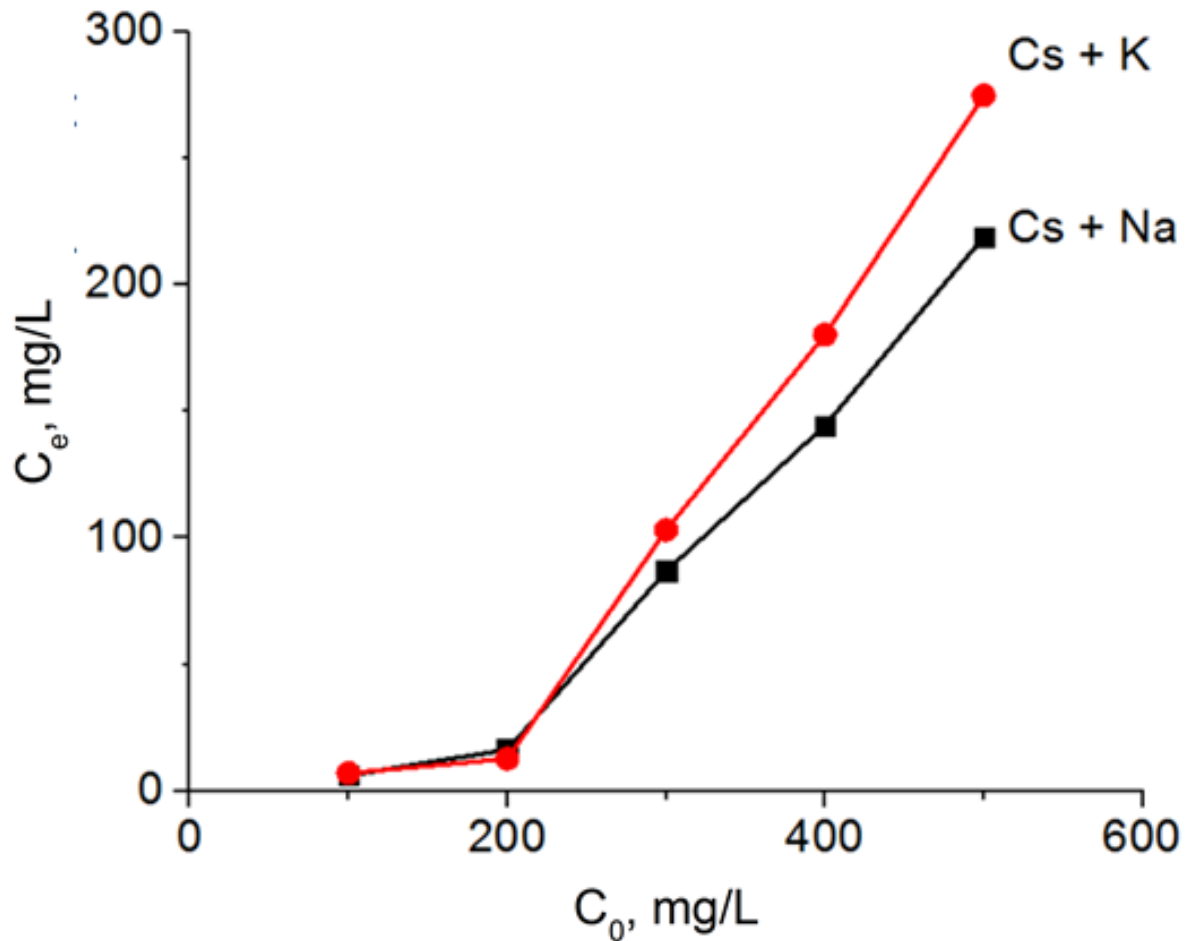


Figure 13: Effect of other alkali metals on Cs^+ adsorption on H-PTA/SiO₂

Adsorption of Strontium and Cobalt

Other possible isotopes formed during nuclear fission are ^{90}Sr and ^{60}Co . As shown in Figure 14, strontium and cobalt demonstrated lower adsorption on H-PTA/SiO₂ with respect to cesium. The adsorption capacity of strontium was 4.6-16.4 mg/g at different initial concentrations of SrCl₂. For CoCl₂, these data were still lower: 2.6-8.5 mg/g. It correlates with

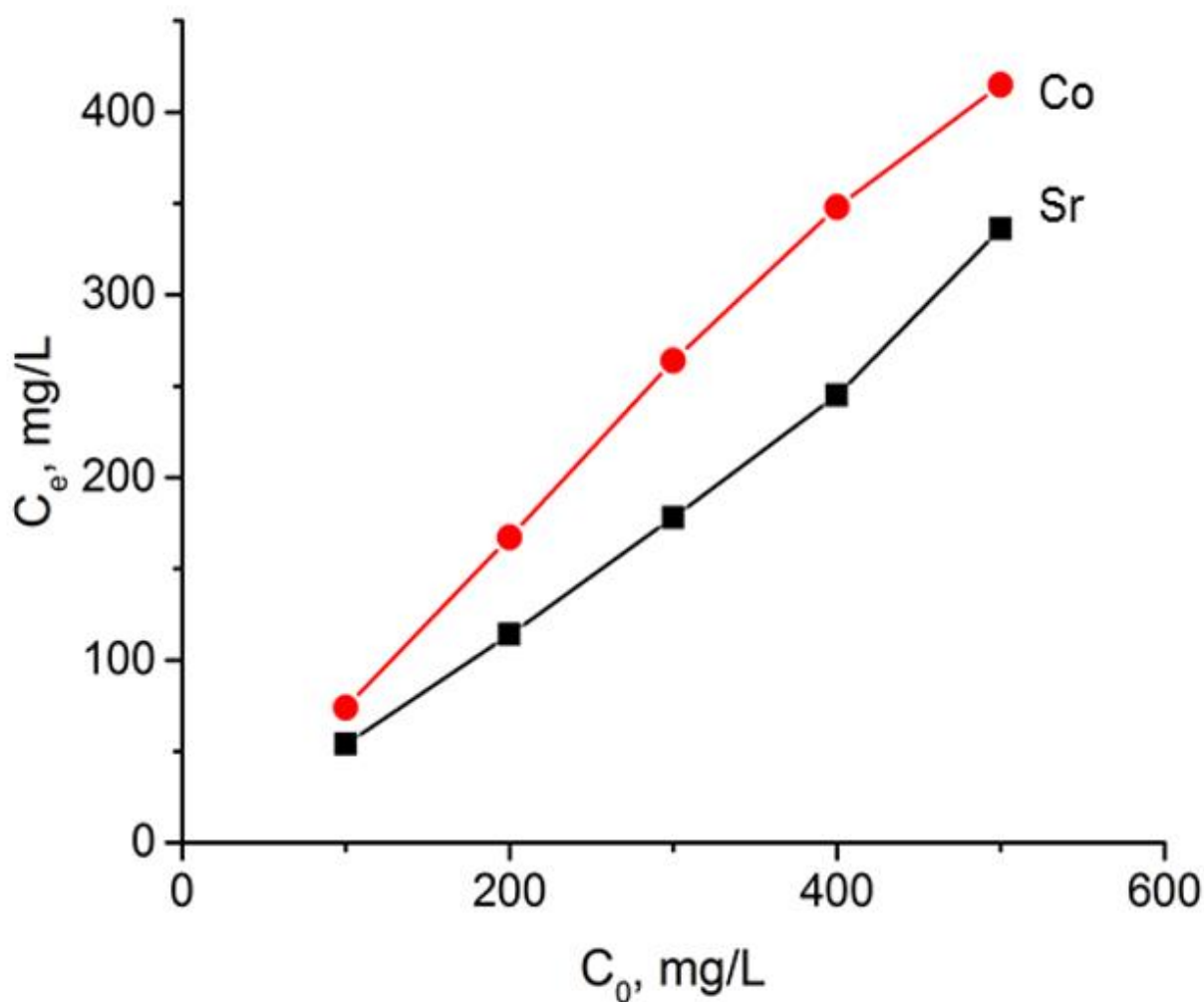


Figure 14: Adsorption of Sr²⁺ and Co²⁺ on H-PTA/SiO₂

the high solubility of Sr₃[PW₁₂O₄₀]₂ and Co₃[PW₁₂O₄₀]₂ in water. Thus the adsorbent can separate ¹³⁷Cs from other radioactive contaminants.

Diffusion Study

Study of the adsorption dependence on contact time showed that this process proceeds in two steps. In the first step, rapid adsorption occurred (Figure 15a). Most of Cs^+ ions were adsorbed during this step. Following this, the adsorption continued at a slower rate.

Based on the data obtained and the nature of highly porous materials, diffusion rates likely play a large role in the overall adsorption of Cs^+ in this case. Using the slope and intercepts of the lines of plots of adsorption (mg/g) vs. $t^{0.5}$ ($\text{min}^{0.5}$), as shown in Figure 15b, the rate constant of intraparticle transport k_{ip} and information related to the thickness of the boundary layer were obtained (presented below in Table 3). As the equilibrium concentration of Cs^+ ions increases, the correlation coefficient of the model as well as the intraparticle diffusion rate increases, showing that intraparticle diffusion plays a larger role in adsorption rate at higher concentrations.

Table 3: Diffusion and Kinetics Data

Initial Cs concentration C_0 , mg/L	Intraparticle diffusion constants			Adsorption kinetic constants			
	k_{id} , mg/(g•min ^{0.5})	C	R^2	k_1 , min ⁻¹	R_1^2	k_2 , g/(mg•min)	R_2^2
100	0.058	8.561	0.571	14.00	0.205	9.056	1
200	0.144	11.891	0.819	3.099	0.765	13.090	0.999
300	0.703	12.074	0.954	0.646	0.940	17.431	0.999
400	1.054	15.235	0.983	0.626	0.895	23.502	0.998
500	1.265	17.972	0.951	0.423	0.992	29.138	0.999

It can be seen from Figure 15a that initial adsorption of Cs^+ ions occurs very quickly, but becomes much slower shortly after. This can be explained by surface sites becoming occupied first before intraparticle adsorption sites. Because of this, diffusion of Cs^+ ions into the pore structure is not necessary at lower concentrations where enough surface sites are available to adsorb most Cs^+ ions. However, at higher concentrations, all surface sites become occupied, so

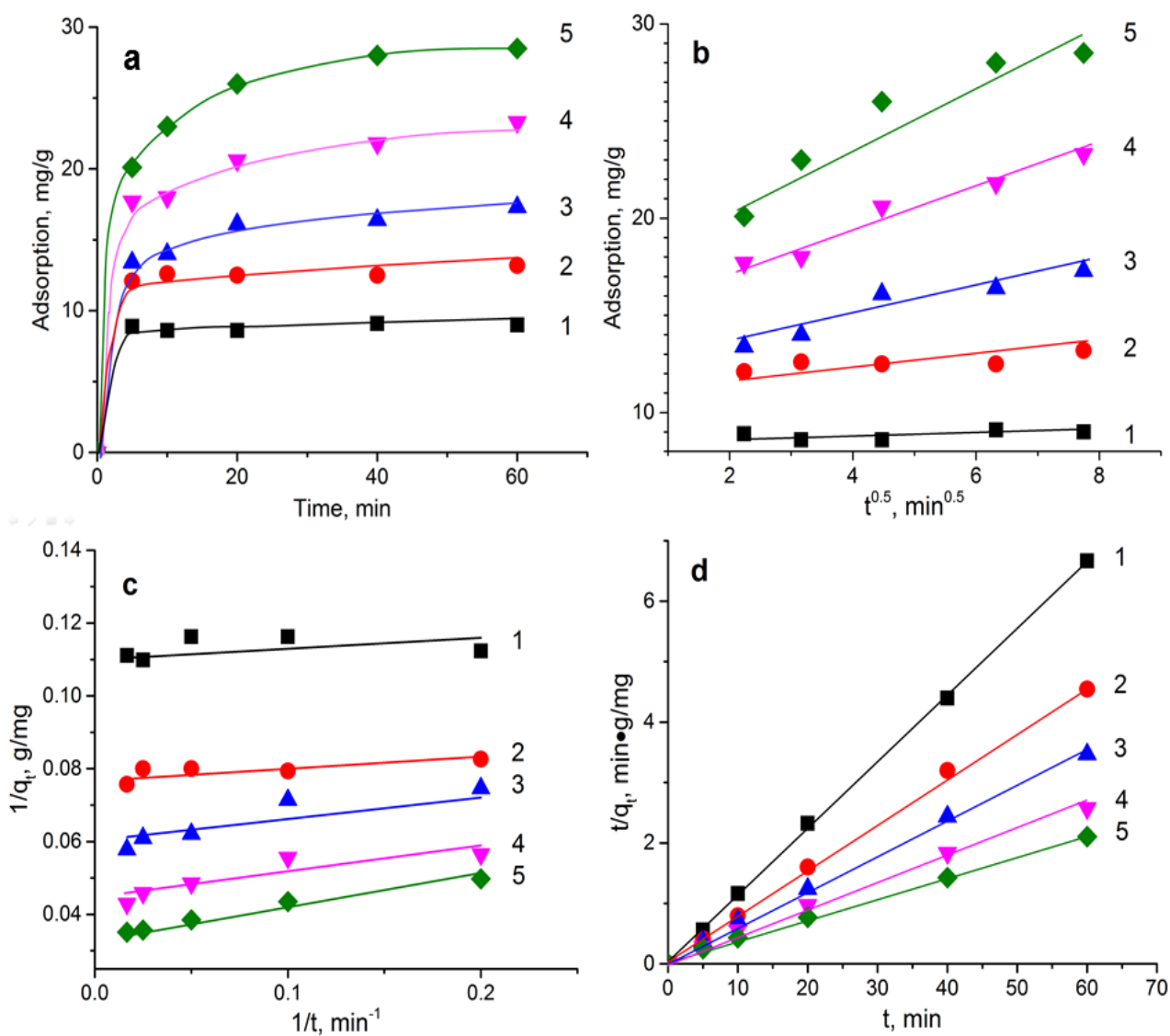


Figure 15: Kinetics of Cs^+ adsorption at different initial concentrations (1 – 100, 2 – 200, 3 – 300, 4 – 400, 5 - 500 mg/L): amount adsorbed vs. time (a), diffusion rate (b), pseudo-first order fitting (c), pseudo-second order fitting (d).

Cs⁺ ions must diffuse into the porous system of the material in order to access additional adsorption sites.

Plots of adsorption vs. $t^{0.5}$ from time-dependent adsorption experiments showed a linear increase of reaction rate with respect to concentration, which is indicative of a pseudo-order process (Figure 16). With this in mind, pseudo-first-order and pseudo-second-order kinetic models were applied to time-dependent adsorption experiments to analyze the adsorption rate of Cs⁺.

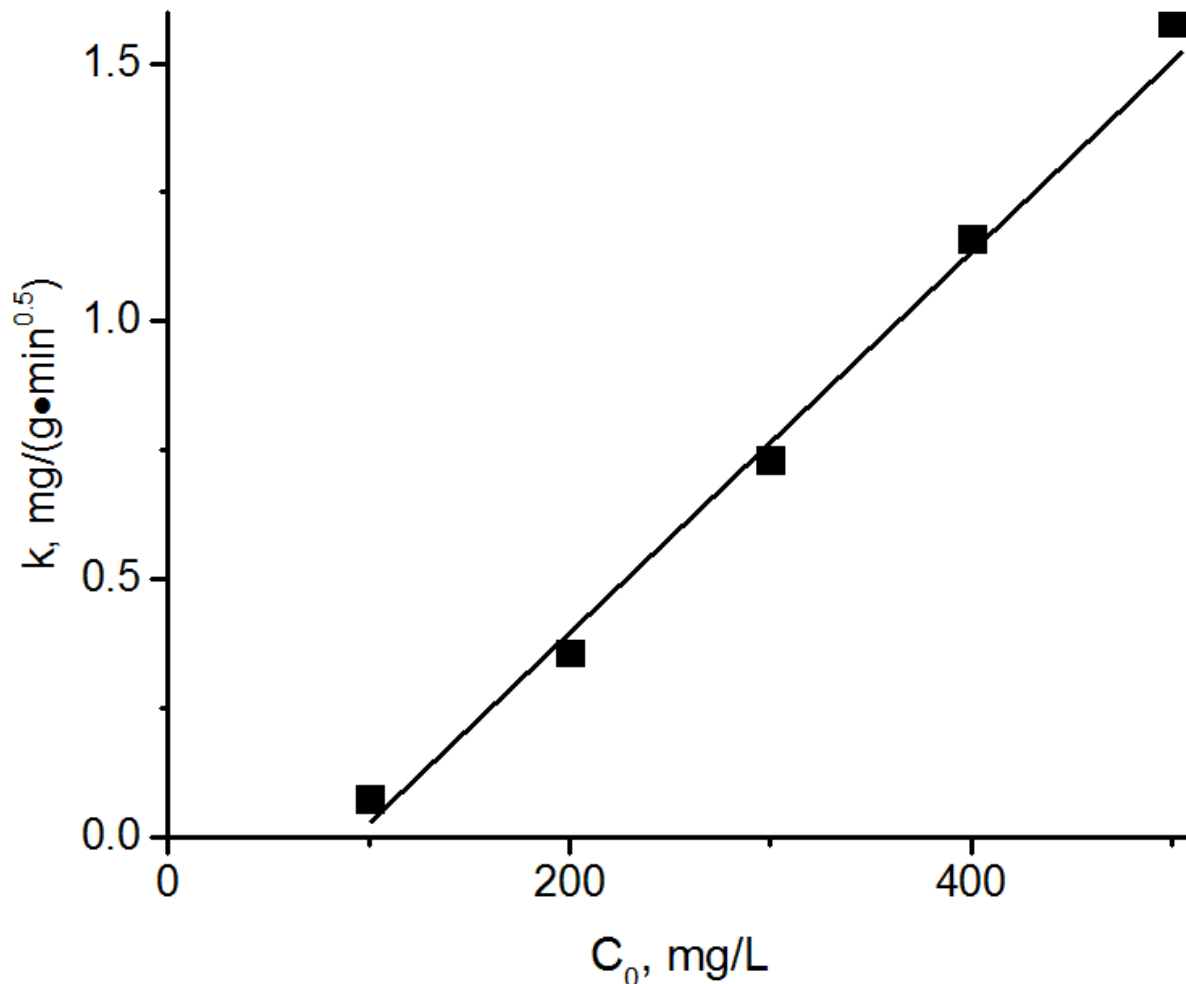


Figure 16: Intraparticle diffusion rate constants at different Cs⁺ concentrations

Correlation coefficients of the pseudo-first-order model (R_1^2) were much lower than the pseudo-second-order model (R_2^2), which implies that the former model does not correctly describe the adsorption process (Figure 15c). However, as shown in Table 3, correlation coefficients for the pseudo-second-order model are all very high, which indicates that the pseudo-second-order model adequately describes the nature of Cs^+ adsorption onto the material (Figure 15d).

Although the overall fit of the pseudo-second-order model was much better than that of the pseudo-first-order, both models showed good agreement at Cs^+ concentrations of 500 mg/L. The pseudo-first-order model assumes that one reactant in a bimolecular chemical reaction is present in high excess, therefore neglecting the concentration of this excess reactant in the rate law. At 500 mg/L of Cs^+ , the concentration of adsorbate molecules is significantly higher than the number of accessible adsorption sites, which results in the pseudo-first-order model showing a higher linearity than at lower concentrations. However, due to the low linearity of the pseudo-first-order model in general, the rate constant of the pseudo-second-order model will be accepted as the true experimental rate constant of the adsorption process.

Column Adsorption Tests

The adsorbent demonstrated high effectiveness at Cs^+ concentrations below 200 mg/L (Figure 17). Cumulative amounts of adsorbed Cs^+ increased with time. In all experiments, adsorption curves were almost linear up to 10-15 mg/g. Following this, the adsorption rate gradually decreased.

The average adsorption rates for different initial concentrations of Cs^+ were calculated by dividing the total amount adsorbed (mg/g) by the time required for adsorption (min). The plot of average adsorption rate vs. concentration (Figure 18) showed a fairly linear relationship,

demonstrating that a flow rate of 1.5 mL/min provides adequate contact time for sufficient intraparticle diffusion required for high adsorption of cesium. The deviations from linearity at higher concentrations of Cs^+ are most likely due to local fluctuations in flow rate, which would result in an inadequate contact time with the adsorbent.

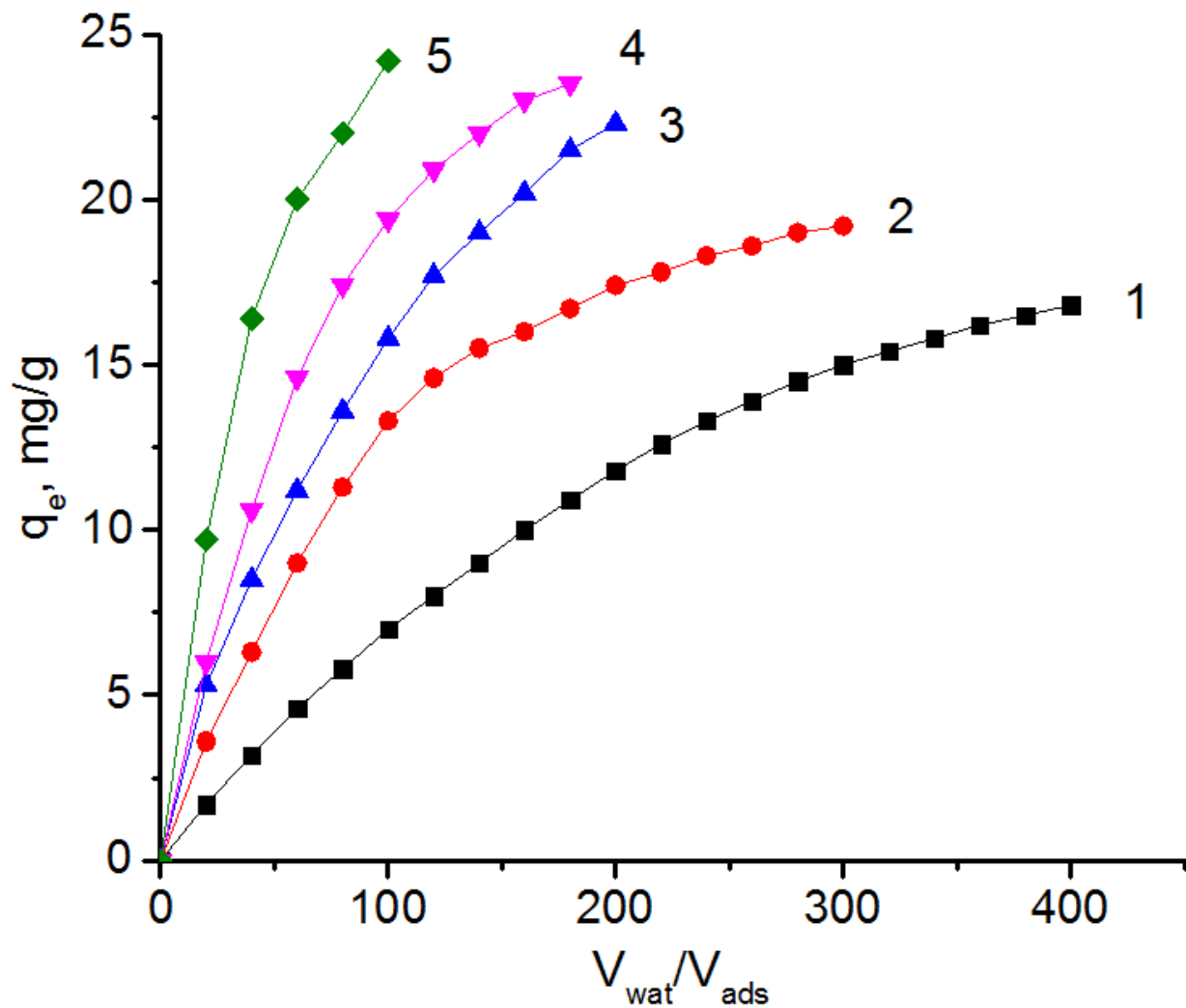


Figure 17: Cumulative adsorption of Cs^+ by H-PTA/SiO₂ in CsCl solution flow at different initial concentrations (1 – 100, 2 – 200, 3 – 300, 4 – 400, 5 – 500 mg/L)

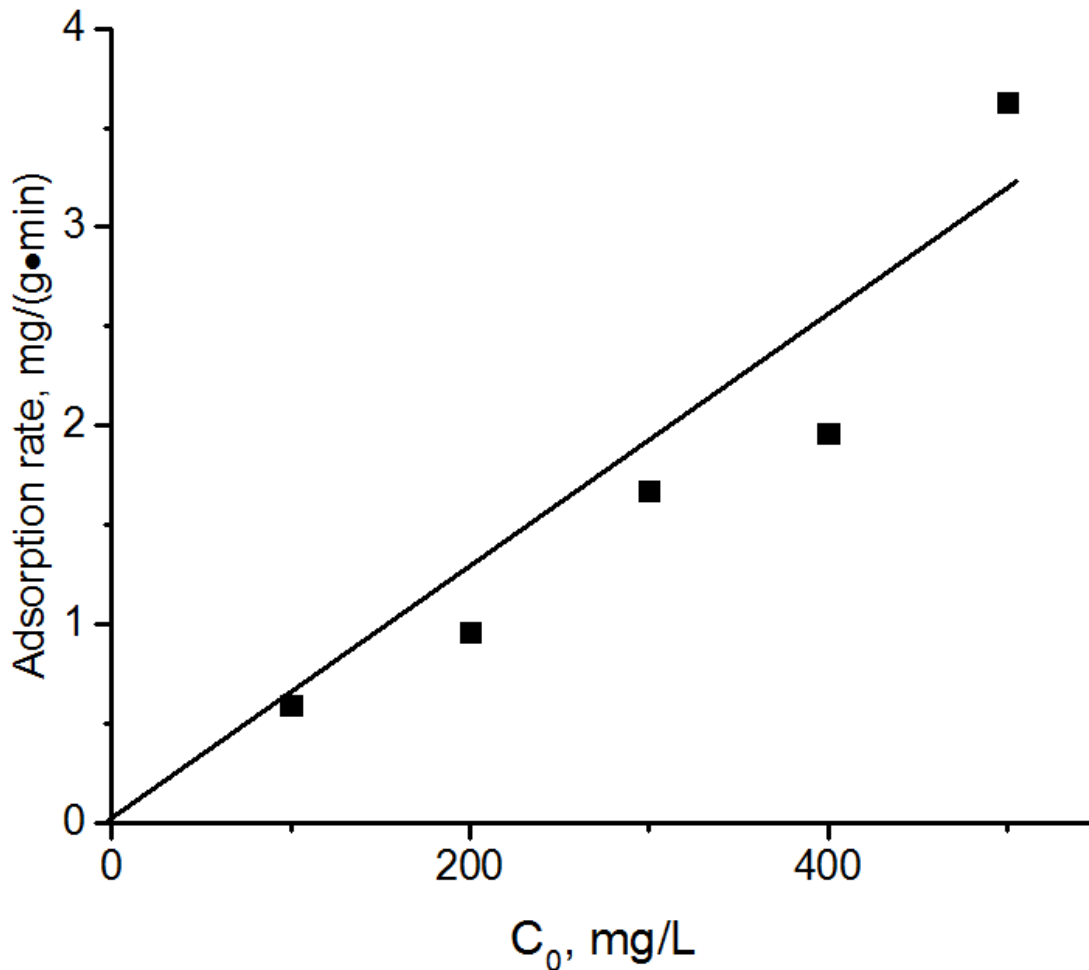


Figure 18: Dependence of the average adsorption rate on the initial Cs^+ concentration

Discussion

Sol-gel synthesis of silica gel in the presence of PTA resulted in the embedding of PTA clusters in the silica network. In the obtained hybrid material, Keggin units were covalently bonded to silicon atoms via oxygen bridges. Covalently bonded Si-O-W was evident from FT-IR spectra (Figure 4) and confirmed by ^{29}Si NMR spectra (Figure 5) as well as the high stability of PTA against leaching. Elemental analysis showed that almost the full amount of PTA used in the reaction was successfully embedded. The volume occupied by one Keggin unit is approximately

0.9 nm³. Considering the data of XRD (Figure 10) and TEM (Figure 7) on the crystallite size, the average cluster of PTA in the silica gel consisted of ≈ 120 Keggin units.

High porosity of the material enabled accessibility of acidic sites located on Keggin units to cations from the solution. The adsorbent pore surface contains two types of acidic sites that can serve as adsorption sites for a base. Strong acidic sites are located on Keggin anions. Their number exceeds the number of acidic hydrogens corresponding to one heteropolyacid anion due to hydration and formation of additional hydronium cations at the surface.⁴³ Evidently from ³¹P NMR (Figure 5) and FT-IR spectra (Figure 4), the anions were highly hydrated. The contents of acidic sites can be determined by titration with a base. However, strong bases decompose Keggin units in aqueous media irreversibly. Thus weak organic bases were used for analysis of acidic sites in anhydrous conditions to prevent PTA hydrolysis. The content of strong sites was found to be 0.09-0.12 sites/nm², depending on accessibility.

The second type of acidic site is represented by silanol groups of silica gel. These sites are extremely weak and may interact only with strong bases. In spite of weakness of these sites, they can serve as adsorption sites for metal cations at certain conditions (Figure 19).

Cesium adsorbed on silanol groups is very unstable and can be removed not only by a weak acid or a base, but also by water. Cs⁺ bonded to surface PTA has a much stronger interaction, however, and is much more difficult to remove.

Study of the adsorption of Cs⁺ on the material surface showed that at room temperature, adsorption occurs on both strong and weak acidic sites. However, at increased temperature only adsorption on strong sites takes place (Figure 12). It is interesting that in the process of adsorption, structural and acidic characteristics of the adsorbent changed. In the Cs-containing material, a significant amount of new micropores formed. As a result, the number of acidic sites

increased. Cs-PTA/SiO₂ contained approximately 0.15 cations/nm² of cesium and 0.15-0.19 acidic sites/nm². This increase in acidity can be attributed to increased microporosity of the sample (Figure 8b).

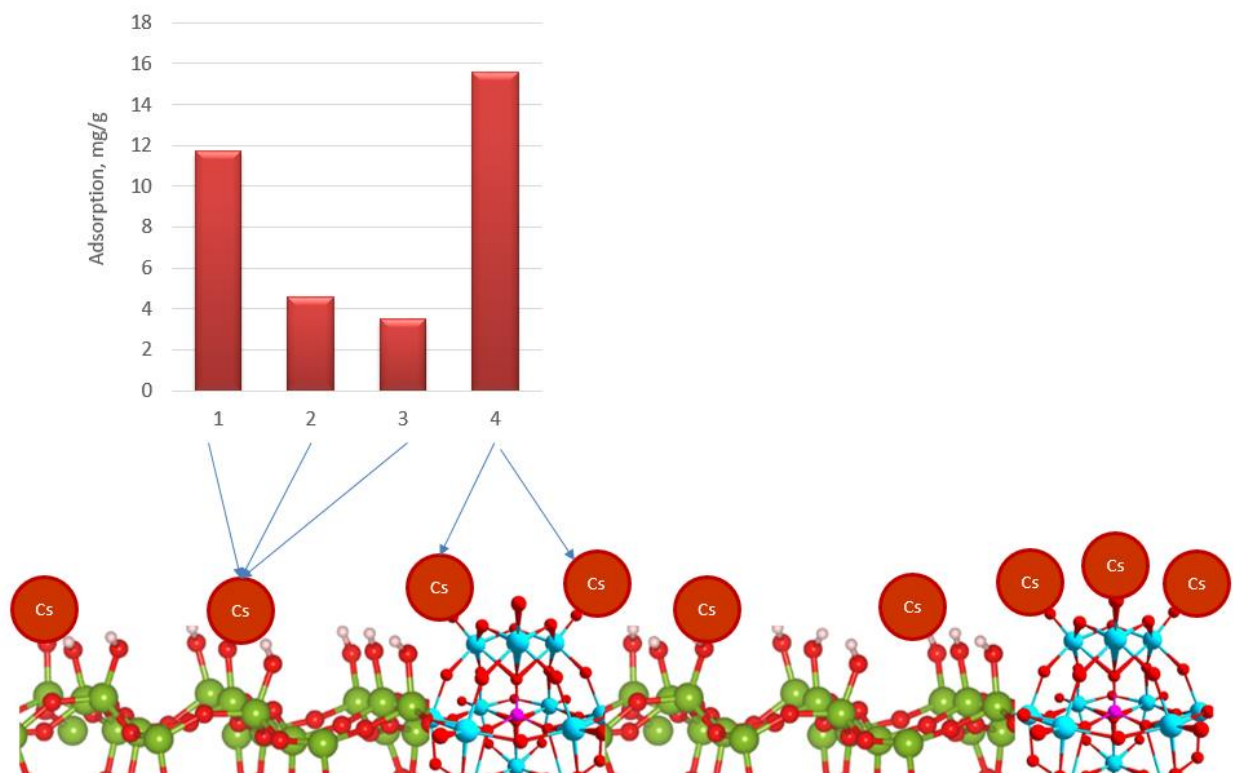


Figure 19: Two types of active adsorption sites for Cs⁺: Silanol groups (1 – water-leachable, 2 – acid-leachable, 3 – base-leachable) and PTA (4 – non-leachable)

Adsorption sites of both types have different accessibility due to their location in the particle structure. High accessibility of external sites provided fast removal of Cs⁺ cations at low concentrations. At higher concentrations, the contribution of internal sites to the total adsorption became more evident. However, intraparticle diffusion limitations make the filling of internal sites by Cs⁺ much slower. As shown by elemental analysis and porosimetry (Table 1 and Figure 8b), a minor portion of acidic sites were not exchanged by Cs⁺ due to steric hindrances in micropores.

A significant advantage of H-PTA/SiO₂ is its stability against leaching. The materials reported earlier obtained by impregnation of silica gel by PTA were unstable in polar solvents due to its high solubility.⁵⁰ The immobilization of PTA by covalent bonding eliminated this drawback.

Conclusions

A hybrid functionalized material containing phosphotungstic acid embedded into a silica network was successfully synthesized. The obtained mesoporous material had high BET surface area and high concentration of surface acidic sites. It demonstrated effectiveness in adsorption of cesium from aqueous solutions. The adsorption occurred on acidic sites of two types. However, at increased temperatures, cesium cations were adsorbed on PTA anions only. Isotherms of adsorption fitted Langmuir and Temkin models. The adsorption proceeded in accordance with the pseudo-second-order rate law. The adsorption of Cs⁺ resulted in notable structural changes in the silica network: formation of new micropores and agglomeration of primary particles. In addition, the formation of new acidic sites was observed. The obtained data could be used in the development of an adsorbent for the removal of radioactive ¹³⁷Cs from nuclear wastes or contaminated water.

REFERENCES

- 1) Starr, S. The Implications of the Massive Contamination of Japan with Radioactive Cesium, In *Proceedings of the Helen Caldicott Foundation Fukushima Symposium*, New York, March 11-12, **2013**.
- 2) Niedree, B., Berns, A., Vereecken, H., Burauel, P. Do Chernobyl-like contaminations with ^{137}Cs and ^{90}Sr affect the microbial community, the fungal biomass and the composition of soil organic matter in soil? *J. Environ. Radioact.* **2009**, 118, 21-29.
- 3) Kocherov, N., Lammer, M., Schwerer, O. *Handbook of Nuclear Data for Safeguards*; International Atomic Energy Agency: Vienna, **1997**.
- 4) Fujimura, S., Muramatsu, Y., Ohno, T., Saitou, M., Suzuki, Y., Kobayashi, T., Yoshioka, K., Ueda, Y. Accumulation of ^{137}Cs by rice grown in four types of soil contaminated by the Fukushima Dai-ichi Nuclear Power Plant accident in 2011 and 2012. *J. Environ. Radioact.* **2015**, 140, 59-64.
- 5) Velasco, H., Cid, A., Anjos, R., Zamboni, C., Rizzotto, M., Valladares, D., Ayub, J. Variability of ^{137}Cs and ^{40}K soil-to-fruit transfer factor in tropical lemon trees during the fruit development period. *J. Environ. Radioact.* **2012**, 104, 64-70.
- 6) Parajuli, D., Takahashi, A., Tanaka, H., Sato, M., Fukuda, S., Kamimura, R., Kawamoto, T. Variation in available cesium concentration with parameters during temperature induced extraction of cesium from soil. *J. Environ. Radioact.* **2015**, 140, 78-83.
- 7) Dushenkov, S., Mikheev, A., Prokhnevsky, A., Ruchko, M., Sorochinsky, B. Phytoremediation of radiocesium-contaminated soil in the vicinity of Chernobyl, Ukraine. *Environ. Sci. Technol.* **1999**, 33, 469-475.

- 8) Rogers, H., Bowers, J., Gates-Anderson, D. An isotope dilution–precipitation process for removing radioactive cesium from wastewater. *J. Hazard. Mater.* **2012**, 243, 124–129.
- 9) Zhang, H., Zhao, X., Wei, J., Li, F. Removal of cesium from low-level radioactive wastewaters using magnetic potassium titanium hexacyanoferrate. *Chem. Eng. J.* **2015**, 275, 262-270.
- 10) Wagh, A., Sayenko, S., Shkuropatenko, V., Tarasov, R., Dykiy, M., Svitlychniy, Y., Virych, V., Ulybkina, E. Experimental study on cesium immobilization in struvite structures. *J. Hazard. Mater.* **2016**, 302, 241-249.
- 11) Han, F., Zhang, G., Gu, P. Removal of cesium from simulated liquid waste with countercurrent two-stage adsorption followed by microfiltration. *J. Hazard. Mater.* **2012**, 225-226, 107-113.
- 12) Zhang, C., Gu, P., Zhao, J., Zhang, D., Deng, Yue. Research on the treatment of liquid waste containing cesium by an adsorption-microfiltration process with potassium zinc hexacyanoferrate. *J. Hazard. Mater.* **2009**, 167, 1057-1062.
- 13) Liu, X., Chen, G., Lee, D., Kawamoto, T., Tanaka, H., Chen, M., Luo, Y. Adsorption removal of cesium from drinking waters: A mini review on use of biosorbents and other adsorbents. *Bioresour. Technol.* **2014**, 160, 142-149.
- 14) Omura, A., Shiozaki, H., Kawamoto, T., Gotoh, A., Kurihara, M., Sakamoto, M., Tanaka, H. Electrochromic thin film of water-dispersible Prussian-blue nanoparticles. *Jpn. J. Appl. Phys. Part 2.* **2008**, 47, 1242-1244.
- 15) Delchet, C., Tokarev, A., Dumail, X., Toquer, G., Barre, Y., Guari, Y., Guerin, C., Larinova, J., Grandjean, A. Extraction of radioactive cesium using innovative functionalized porous materials. *RSC Adv.* **2012**, 2, 5707-5716.

- 16) Thammawong, C., Opaprakasit, P., Tangboriboonrat, P., Sreearunothai, P. Prussian blue-coated magnetic nanoparticles for removal of cesium from contaminated environment. *J. Nanopart. Res.* **2013**, 15, 1689-1698.
- 17) Chen, G., Chang, Y., Liu, X., Kawamoto, T., Tanaka, H., Parajuli, D., Chen, M., Lo, Y., Lei, Z., Lee, D. Prussian blue non-woven filter for cesium removal from drinking water. *Sep. Purif. Technol.* **2015**, 153, 37-42.
- 18) Kozhevnikov, I. V. Heterogeneous Catalysis by Heteropoly Compounds. In *Polyoxometalate Molecular Science*; Borrás-Almenar, J.J., Coronado, E., Müller, A., Pope, M. Eds.; Kluwer Academic Publishers: Dordrecht, Netherlands, **2003**; pp. 351-380.
- 19) Ono, Y., *Heteropolyacid Catalysis-a unique Blend of Acid-Base and Redox Properties*; Perspectives in Catalysis: Chemistry for the 21st Century, Thomas, J.M. and Zamaraev, K.I., Eds., Blackwell Scientific: Oxford, **1992**, pp. 431-463.
- 20) Kozhevnikov, I. Catalysts by heteropoly acids and multicomponent polyoxometalates in liquid-phase reactions. *Chem. Rev.* **1998**, 98, 171-198.
- 21) Lopez, X., Bo, C., Poblet, J. Relative stability in α and β -Wells–Dawson heteropolyanions: A DFT study of $[P_2M_{18}O_{62}]^{n-}$ (M = W and Mo) and $[P_2W_{15}V_3O_{62}]^{n-}$. *Inorg. Chem.* **2003**, 42, 2634-2638.
- 22) Rafiee, E., Kahrizi, M. Cesium salts of phosphotungstic acid: comparison of surface acidity, leaching stability and catalytic activity for the synthesis of β -ketoenol ethers. *S. Afr. J. Chem.*, **2013**, 66, 145-149.
- 23) Na, K. Okuhara, T. Misono, M. Skeletal isomerization of n-butane over caesium hydrogen salts of 12-tungstophosphoric acid. *J. Chem. Soc.* **1995**, 91, 367-373.

- 24) Bardin, B., Bordawekar, S., Neurock, M., Davis, R. Acidity of Keggin-type heteropolycompounds evaluated by catalytic probe reactions, sorption calorimetry, and density functional quantum chemical calculations. *J. Phys. Chem. B.* **1998**, 102, 10817-10825.
- 25) Newman, A.D., Lee, A.F., Wilson, K., Young, N.A. On the active site in H₃PW₁₂O₄₀/SiO₂ catalysts for fine chemical synthesis. *Catal. Lett.* **2005**, 102, 45-50.
- 26) Kukovecz, A., Balogi, Z., Konya, Z., Toba, M., Lentz, P., Niwa, S.-I., Mizukami, F., Molnar, A., Nagy, J.B., Kirisci, I. Synthesis, characterization and catalytic applications of sol-gel derived silica-phosphotungstic acid composites. *Appl. Catal., A: General* **2002**, 228, 83-94.
- 27) Yang, L., Qi, Y., Yuan, X., Shen, J., Kim J. Direct synthesis, characterization and catalytic application of SBA-15 containing heteropolyacid H₃PW₁₂O₄₀. *J. Mol. Catal.* **2005**, 229, 199-205.
- 28) Guo, Y., Li, K., Yu, X., Clark, J. H. Mesoporous H₃PW₁₂O₄₀-silica composite: Efficient and reusable solid acid catalyst for the synthesis of diphenolic acid from levulinic acid. *Appl. Catal., B: Environmental.* **2008**, 81, 182-191.
- 29) Li, K., Hu, J., Li, W., Ma, F., Xu, L., Guo, Y. Design of mesostructured H₃PW₁₂O₄₀-silica materials with controllable ordered and disordered pore geometries and their application for the synthesis of diphenolic acid. *J. Mater. Chem.* **2009**, 19, 8628-8638.
- 30) Dafaud, V., Lefebvre, F. Inorganic hybrid materials with encapsulated polyoxometallates. *Materials*, **2010**, 3, 682-703.
- 31) Fahlman, B. *Materials Chemistry*, 2nd ed.; Springer: New York, **2011**.
- 32) Tolbert, S. Mesoporous silica: Holey quasicrystals. *Nature Materials*, **2012**, 11, 749-751.

- 33) Adetola, O., Golovko, L., Vasiliev, A. Modification of silica gel by heteropolyacids. *Key Eng. Mater.* **2016**, 689, 126-132.
- 34) Sandesh, S., Manjunathan, P. Halgeri, A.B., Shanbhag, G.V. Glycerol acetins: fuel additive synthesis by acetylation and esterification of glycerol using cesium phosphotungstate catalyst. *RSC Adv.* **2015**, 5, 104354-104362.
- 35) Okuhara, T., Mizuno, N., Misono, M. Catalytic chemistry of heteropoly compounds. *Adv. Catal.* **1996**, 41, 113-252.
- 36) Zhang, R., Yang, C. A novel polyoxometalate-functionalized mesoporous hybrid silica: synthesis and characterization. *J. Mater. Chem.* **2008**, 18, 2691-2703.
- 37) Cypryk, M., Apeloig, Y. Mechanism of the acid-catalyzed Si-O bond cleavage in siloxanes and siloxanols. A theoretical study. *Organometallics*, **2002**, 21, 2165-2175.
- 38) Luzgin, M.V., Kazantsev, M.S., Volkova, G.G., Stepanov, A.G. Solid-state NMR study of the kinetics and mechanism of dimethyl ether carbonylation on cesium salt of 12-tungstophosphoric acid modified with Ag, Pt, and Rh. *J. Catal.* **2013**, 308, 250-257.
- 39) Wang, Z., Navarrete, J. Keggin structure and surface acidity of 12-phosphotungstic acid grafted Zr-MCM-48 mesoporous molecular sieves. *WJNSE* **2012**, 2, 134-141.
- 40) Okuhara, T., Nishimura, T., Watanabe, H., Misono, M. Insoluble heteropoly compounds as highly active catalysts for liquid-phase reactions. *J. Mol. Catal.* **1992**, 74, 247-256.
- 41) Weiss Jr., C.A., Kirkpatrick, R.J., Altaner, S.P. The structural environments of cations adsorbed onto clays: ¹³³Cs variable-temperature MAS NMR spectroscopic study of hectorite. *Geochim. Cosmochim. Acta.* **1990**, 54, 1655-1669.
- 42) Dias, J.A., Caliman, E., Dias, S.C.L. Effects of cesium ion exchange on acidity of 12-tungstophosphoric acid. *Microporous Mesoporous Mater.* **2004**, 76, 221-232.

- 43) Okuhara, T., Tatematsu, S., Lee, K.Y., Misono, M. Catalysis by heteropoly compounds. XII. Adsorption properties of 12-tungstophosphoric acid and its salts. *Bull. Chem. Soc. Jpn.* **1989**, 62, 717-723.
- 44) Xiao, Y., Xiang, Y., Xiu, R., Lu, S. Development of cesium phosphotungstate salt and chitosan composite membrane for direct methanol fuel cells. *Carbohydr. Polym.* **2013**, 98, 233–240.
- 45) Okuhara, T., Watanabe, H., Nishimura, T., Inumaru, K., Misono, M. Microstructure of cesium hydrogen salts of 12-tungstophosphoric acid relevant to novel acid catalysis. *Chem. Mater.* **2000**, 12, 2230-2238.
- 46) Jewett, J.R., Jensen, L. Assessment of available particle size data to support an analysis of the waste feed delivery system transfer system. Report RPP-6247, U.S. Department of Energy, **2000**.
- 47) Olejniczak, Z., Sulikowski, B., Kubacka, A., Gasiór, M. Heterogenization of 12-tungstophosphoric acid on stabilized zeolite Y. *Top. Catal.* **2000**, 11/12, 391–400.
- 48) Marosi, L., Platero, E.E., Cifre, J., Arean, C.O. Thermal dehydration of $H_{3+x}PV_xM_{12-x}O_{40} \cdot yH_2O$ Keggin type heteropolyacids; formation, thermal stability and structure of the anhydrous acids $H_3PM_{12}O_{40}$, of the corresponding anhydrides $PM_{12}O_{38.5}$ and of a novel trihydrate $H_3PW_{12}O_{40} \cdot 3H_2O$. *J. Mater. Chem.* **2000**, 10, 1949-1955.
- 49) Yang, X., Shen, X., Jing, M., Liu, R., Lu, Y., Xiang, J. Removal of heavy metals and dyes by supported nano zero-valent iron on barium ferrite microfibers. *J. Nanosci. Nanotechnol.* **2014**, 14, 5251–5257.

50) Yuan, C., Zhang, F., Wang, J., Ren, X. 12-Phosphotungstic acid and its Cs salt supported on various porous carriers as catalysts for the synthesis of fructose. *Catal. Commun.* **2005**, 6, 721–724.

VITA

KENNETH SEATON

Education: M.S. East Tennessee State University, Johnson City, TN (May, 2017)
Adsorption of Cesium on Phosphotungstic Acid Imbedded in Silica Matrix
Research Advisor: Aleksey Vasiliev

B.S. East Tennessee State University Johnson City, Tennessee, US
(December, 2014)
Research Advisor: Aleksey Vasiliev

Employment: Eastman Chemical Company, Kingsport, TN (May 2014 – August 2015)
Laboratory Analyst
Job duties: routine quality control analysis of chemicals utilizing gas chromatography as well as maintaining and calibrating instruments, interpreting GC chromatograms in order to determine content of samples, and adhering to proper safety standards set by Eastman. Proficiency acquired: the skill required to operate and maintain a gas chromatographer and skills in preparing industry grade standards for lab use.

Teaching: East Tennessee State University (August 2015 – May 2017)
Teaching Assistant
Teaching Duties: Laboratory sections in General Chemistry I, General Chemistry II, Introductory Integrated Lab, Organic Chemistry I and Organic Chemistry II. Duties include preparing and presenting pre-laboratory lectures in order to introduce or reinforce core concepts in chemistry, grading assignments and maintaining an accurate gradebook, assisting students in lab work during experiments, helping students with coursework during office hours, and ensuring a friendly and safe environment for students to learn and experience chemistry.

ETSU Upward Bound Program (June 2016 – July 2016)
Chemistry Instructor
Teaching Duties: Managing classrooms of students, preparing and presenting lectures for Chemistry I and Chemistry II classes, writing and grading exams as well as daily classwork, maintaining a gradebook, preparing and supervising laboratory experiments, and conveying basic concepts in chemistry to introductory-level high school chemistry students.

Honors/Awards: Outstanding Teaching Assistant Award – East Tennessee State University, 2016

Publications:

- 1) Brown L., Seaton K., Mohseni R., Vasiliev A. Immobilization of heavy metals on pillared montmorillonite with a grafted chelate ligand. *J. Hazard. Mater.* **2013**, 261, 181–187.
- 2) Appiah-Kubi G., Seaton K., Vasiliev A. Functionalization of silica surface using Chan–Lam coupling, *Tetr. Lett.* **2014**, 55, 2722-2726.
- 3) Seaton, K., Little, I., Tate, C., Mohseni, R., Roginskaya, M., Volodymyr, P., Vasiliev, A. Adsorption of cesium on phosphotungstic acid imbedded in silica matrix. *Microporous Mesoporous Mater.* **2017**, 244, 55-66.

Presentations:

- 1) Seaton K., Little I., **Vasiliev A.** Adsorption of caesium on porous silica gel modified by phosphotungstic acid, *5th Int. Conf. Multifunctional, Hybrid and Nanomaterials*, Lisbon, Portugal 2017, abstr. P1.185
- 2) Seaton K., Little I., **Vasiliev A.** Efficient adsorbent for immobilization of caesium on contaminated areas. *5th World Congress on Materials Science & Engineering*, Alicante, Spain, 2016. Abstr. publ. in: *Journal of Material Science and Engineering* 2016, v.5, p. 85 (suppl.)
- 3) **Seaton K.**, Little I., Vasiliev A. *Adsorption of caesium from contaminated waters on phosphotungstic acid embedded in silica matrix.* 68th Southeastern Regional ACS Meet., Columbia, SC, 2016, 821.
- 4) **Kubi G.**, Seaton K., Vasiliev A. *Application of Chan-Lam coupling for surface modification.* Appalachian Student Research Forum, Johnson City, TN, 2014, p. 53.
- 5) **Seaton K.**, Kubi G., Vasiliev A. *Functionalization of surface using N-arylation.* Abstr. 46th Southeast Undergraduate Research Conference, Knoxville, TN, 2014, p. 18.
- 6) **Seaton K.** *Application of Chan-Lam coupling for surface functionalization.* ETSU Boland Undergraduate research symposium, Johnson City, TN, 2014.
- 7) Kubi G., Seaton K., **Vasiliev A.** *Functionalization of surface by catalytic N-arylation.* 245th ACS Nat. Meet., Dallas, TX, 2014, abstr. COLL-142.
- 8) Brown L., Seaton K., **Vasiliev A.** *Immobilization of heavy metals in contaminated soils and sludge using pillared organoclay.* 245th ACS Nat. Meet., New Orleans, LO, 2013, abstr. INOR-403.
- 9) **Brown L.**, Seaton K., Vasiliev A. *Application of pillared organoclay for immobilization of heavy metals in contaminated soils.* Appalachian Student Research Forum, Johnson City, TN, 2013, p. 42-43.

*presenters identified in bold

Grants:

- 1) Kenneth Seaton and Aleksey Vasiliev, Student Faculty Collaborative Grant, *Functionalization of Silica Surface using Chan-Lam Coupling*, Funded for \$1200 in Fall of 2013.